


## Article

# Resource Optimization Using a Step-by-Step Scheme in Wireless UWB Sensing and Localization Networks <sup>†</sup>

Ruihang Zhang <sup>1</sup> , Jiayan Yang <sup>1</sup>, Mu Jia <sup>1</sup>, Tingting Zhang <sup>1</sup> and Yachuan Bao <sup>2,3,\*</sup>
<sup>1</sup> School of Electronics and Information Engineering, Harbin Institute of Technology, Shenzhen 518055, China; 190210523@stu.hit.edu.cn (R.Z.); 21b352008@stu.hit.edu.cn (J.Y.); 20s152109@stu.hit.edu.cn (M.J.); zhangtt@hit.edu.cn (T.Z.)

<sup>2</sup> State Key Laboratory of Satellite Navigation System and Equipment Technology, Shijiazhuang 050081, China

<sup>3</sup> The 54th Research Institute of China Electronics Technology Group Corporation, Shijiazhuang 050081, China

\* Correspondence: baoyachuan@126.com

<sup>†</sup> This paper is an extended version of our paper published in Zhang, R.; Yang, J.; Zhang, T. Resource Optimization in Time-Varying Wireless Sensing and Localization Networks. In Proceedings of the 2023 IEEE 97th Vehicular Technology Conference (VTC2023-Spring), Florence, Italy, 20–23 June 2023; pp. 1–6.

**Abstract:** Wireless localization and target sensing both rely on precise extraction of parameters such as signal amplitude, propagation delay, and Doppler shift from the received signals. Due to the high multi-path resolution and strong penetration, both localization and sensing can be achieved through identical UWB waveforms. In this paper, we try to properly allocate resources for localization and sensing to fully exploit the potential of UWB systems. Considering the complexity of the multi-slot networks, we derive the Fisher Information Matrix (FIM) expressions for single-slot and dual-slot integrated sensing and localization (ISAL) networks, respectively, and propose two resource optimization schemes, namely the step-by-step scheme and the integrated scheme, respectively. The numerical results show that: (i) for the sensing-resource-limited networks with relatively uniform node distribution, the energy allocated to each step in the step-by-step scheme satisfies the relationship energy for clock offset < energy for radar localization < energy for target sensing; (ii) in the multi-slot ISAL networks, more energy will be allocated to the time slots where the networks are relatively sensing-resource-limited; (iii) the step-by-step scheme is more suitable for the sensing-resource-abundant networks, while the integrated scheme is more suitable for the sensing-resource-limited networks.

**Keywords:** integrated sensing and localization; clock offset; spatiotemporal cooperation; Fisher information; resource optimization allocation



**Citation:** Zhang, R.; Yang, J.; Jia, M.; Zhang, T.; Bao, Y. Resource Optimization Using a Step-by-Step Scheme in Wireless UWB Sensing and Localization Networks. *Appl. Sci.* **2024**, *14*, 2665. <https://doi.org/10.3390/app14062665>

Academic Editor: Alessandro Lo Schiavo

Received: 25 December 2023

Revised: 5 February 2024

Accepted: 5 February 2024

Published: 21 March 2024



**Copyright:** © 2024 by the authors. Licensee MDPI, Basel, Switzerland. This article is an open access article distributed under the terms and conditions of the Creative Commons Attribution (CC BY) license (<https://creativecommons.org/licenses/by/4.0/>).

## 1. Introduction

### 1.1. Background and Motivation

With the development of the Internet of Things (IoTs) and massive machine type communications (mMTCs), more and more wireless devices require connections [1]. The surge in the number of wireless devices has led to a shortage of wireless spectrum resources. In recent years, people have found that reusing the functions of wireless communication networks has many advantages, such as improving spectrum efficiency and reducing hardware equipment costs [2]. Traditional radar positioning networks typically include two types of nodes: anchors with known positions and radars with unknown positions. The positions of radars are determined through measurements from other active radars and anchors, including time of arrival (TOA) [3,4], time difference of arrival (TDOA) [5,6], angle of arrival (AOA) [7,8], received signal strength (RSS) [9,10], and so on. In addition to active positioning, this paper also conducts research on passive sensing, where positions of the targets can be determined through time sum of arrival (TSOA) [11,12]. The realization of wireless localization and sensing relies on accurately extracting relevant parameters such

as signal amplitude, propagation delay, and Doppler shift from the received signals, and both can be achieved with high accuracy through UWB waveforms [13]. The similarity between wireless localization and target sensing provides a prerequisite for the integration of localization and sensing networks.

Due to the fact that both wireless localization and target sensing are parameter estimation issues, before designing a parameter estimation algorithm for wireless localization or target sensing, we need to first obtain the theoretical estimation error lower bound to benchmark the accuracy of the designed algorithm. The authors in [14] show that inter-node measurements and intra-node measurements can bring spatial and temporal cooperation gains to the accuracy of localization systems, respectively. In addition, due to the fact that practical networks are often resource-constrained, in order to improve the accuracy of localization and sensing as much as possible, it is necessary to optimize the allocation of resources in the networks.

### 1.2. Related Works

Localization and positioning will be interchangeably used for estimation of the state (position, orientation) of a connected device in a global frame of reference [15]. For the investigations of wireless localization, the authors in [16] show that the Cramer–Rao lower bound (CRLB) is commonly used as the lower bound of the variance of unbiased estimation parameters in wireless localization networks. The authors in [17] introduce some basic concepts such as FIM, equivalent Fisher information matrix (EFIM), and so on, and also provide the derivation of the localization FIM expressions in wireless localization networks. The authors in [18] provide analysis for the error lower bound of localization in non-cooperative and spatial cooperative wireless localization networks, respectively. For radar localization networks that have difficult-to-meet trilateration, a method is provided to assist anchors by mutual ranging between radars to achieve accurate localization of radars. The authors in [14] provide specific FIM expressions of non-cooperative, spatial cooperative, and spatiotemporal cooperative wireless localization networks, respectively. It also provides another two lower bounds—the Ziv–Zakai Lower Bound and the Weiss–Weinstein Lower Bound—and compares their performance with traditional CRLB’s performance in wireless localization networks. The authors in [19] focus on the localization performance bound in uplink massive MIMO with few-bit ADCs. They elucidate that massive MIMO equipped with low-resolution ADCs can still achieve high-precision localization performance. Additionally, the desired localization CRLB is also derived, guiding the design for localization in quantized massive MIMO.

Compared with localization and positioning, sensing has a broader scope, from channel parameter estimation and carrier sensing to presence detection [20]. For the investigations of target sensing, the authors in [15] discuss the geometric information brought by the different components in the sensing channel decomposition, such as channel gain, AOA angle, TSOA delay, and so on. The authors in [21] state the impossibility of equipping each target with communication devices in some circumstances, such as intrusion detection and wildlife monitoring, and propose an inexpensive and efficient target sensing approach called RSS distribution-based localization (RDL), compared with other target sensing techniques, such as GPS and channel state information (CSI) [22]. Although the aforementioned achievements include the geometric information of the sensing links and the implementation methods of target sensing, there is little research with respect to analysis of the fundamental limits in target sensing networks. So far, the majority of research on fundamental limits has focused on wireless localization networks, and there is still little research on the fundamental limits of ISAL networks.

In terms of research on network resource optimization, the authors in [23] propose power optimization schemes between nodes for wireless localization networks and target sensing networks, respectively. The authors in [24] show that, in wireless localization networks, the problem of anchor power optimization can be transformed into a semi-definite program (SDP), and specific SDP solutions are provided. The authors in [25]

find the regularity of node power optimization in single-slot synchronous ISAL networks, indicating that, in order to minimize target sensing error in the power-limited networks when the anchor power allocation in the network remains unchanged, more power will be allocated to the radars closer to the target. Additionally, in [25], the optimization of power in ISAL networks is achieved by simultaneously optimizing all the variables. However, when the number of variables is large, the optimization problem is often too complicated to solve. Therefore, we need to explore a new optimization solution, and there has been no relevant research on this issue so far.

### 1.3. Main Contributions

The main contributions of this paper are as follows.

- We propose some new ISAL system models, namely, the dual-slot synchronous ISAL network with spatiotemporal cooperation, the single-slot asynchronous ISAL network with spatial cooperation, and the dual-slot asynchronous ISAL network with spatiotemporal cooperation.
- We provide the derivation of corresponding FIM expressions for single-slot and dual-slot asynchronous ISAL networks, pointing out that the proposed RLM-OWR method can introduce temporal cooperation between the estimation of clock offsets in two time slots in the dual-slot asynchronous ISAL networks.
- We propose a step-by-step resource allocation scheme, which transforms the multi-parameter optimization problem into multiple sequential optimization problems with a single parameter, avoiding the difficulty caused by simultaneously dealing with too many parameters when solving optimization problems. We also propose an improvement method from the perspective of energy allocation to solve the problem of the high time complexity of the step-by-step scheme. By comparing the optimization results of the step-by-step scheme and the traditional integrated scheme, we summarize the suitable scenarios of each scheme.

**Notations:** We use lowercase and uppercase bold symbols to denote vectors and matrices, respectively. The lowercase bold subscript symbols (e.g.,  $\mathbf{a}$  in  $(\mathbf{A})_{\mathbf{a}}$ ) represent the operation of taking the submatrix corresponding to the parameter vector (i.e.,  $\mathbf{a}$  in the example) from the matrix (i.e.,  $\mathbf{A}$  in the example). The notation  $\|\cdot\|$  is the Euclidean norm of its argument;  $\text{tr}(\cdot)$  is the trace of a square matrix;  $\mathbb{E}(\cdot)$  is the expectation operator of its argument;  $|\cdot|$  represents the cardinality of the set;  $\mathbf{A} \succeq \mathbf{B}$  denotes that the matrix  $\mathbf{A} - \mathbf{B}$  is positive semi-definite.

## 2. System Model

When it comes to the system model of localization and sensing, there are four types of networks to be discussed, namely, wireless localization networks, target sensing networks, single-slot static ISAL networks [25], and multi-slot dynamic ISAL networks. Considering the complexity of the multi-slot networks, this part discusses the dual-slot ( $N = 2$ ) dynamic ISAL networks instead [26].

The general system description can be seen in Figures 1–4. Assume that there are  $N_a$  anchors,  $N_r$  radars, and  $N_t$  targets in each network, where the anchors' positions are known and determined. In the dual-slot dynamic ISAL networks, the radars' and targets' positions remain unchanged in a single time slot but change in different time slots. Anchors and radars called active nodes are both considered to be able to transmit and receive signals, while targets called passive nodes can only reflect signals.

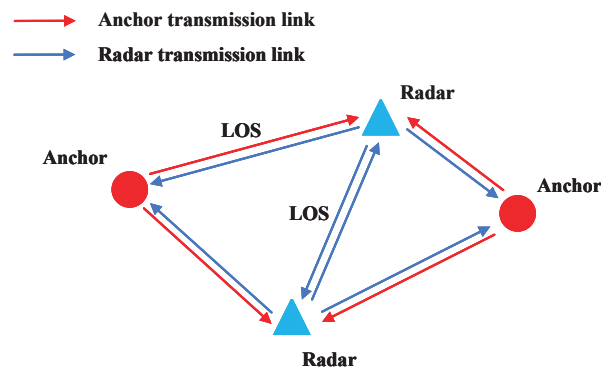


**Figure 1.** Wireless localization system model with spatial cooperation, where the solid red and blue lines, respectively, represent the anchor transmission link and the radar transmission link.

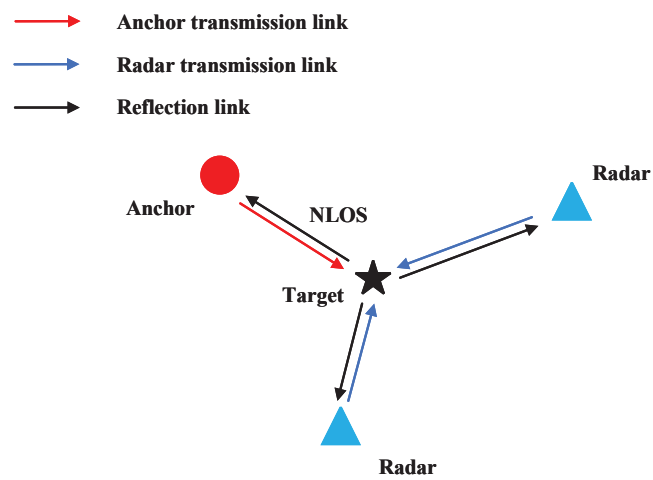


**Figure 2.** Target sensing system model, where the solid red, blue, and black lines, respectively, represent the anchor transmission link, the radar transmission link, and the reflection link.

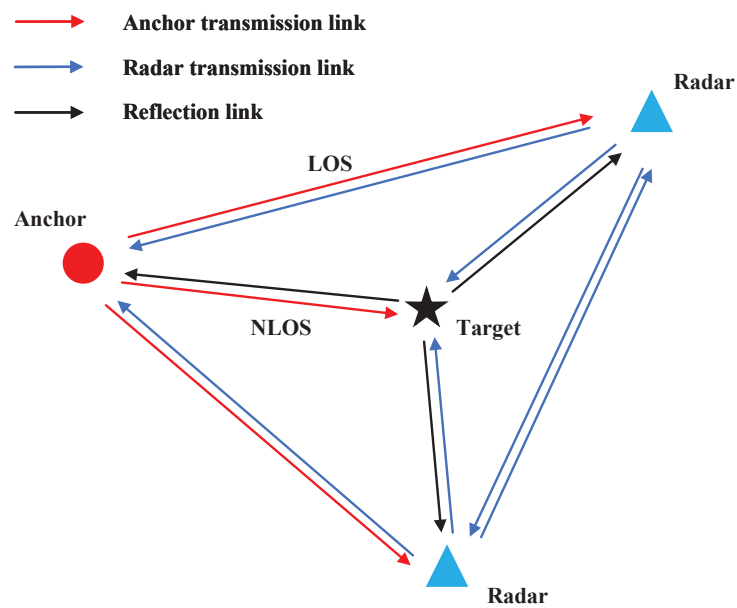


**Figure 3.** ISAL system model with spatial cooperation, where the solid red, blue, and black lines, respectively, represent the anchor transmission link, the radar transmission link, and the reflection link.

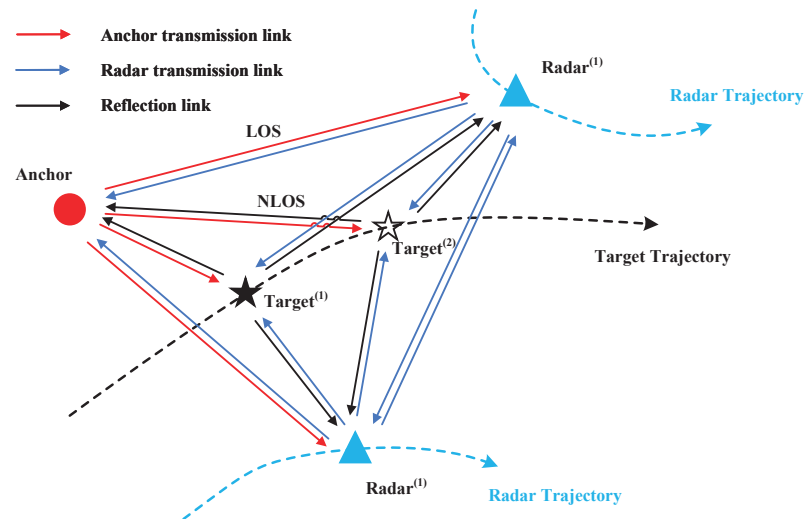


**Figure 4.** ISAL system model with spatiotemporal cooperation, where the solid red, blue, and black lines, respectively, represent the anchor transmission link, the radar transmission link, and the reflection link. The dashed black line and the dashed blue line are, respectively, the trajectories of the moving target and radars. The superscript  $(n)$ ,  $n = 1, 2, \dots, N$  represents the  $n$ th time slot.

### 2.1. Wireless Localization Network

As shown in Figure 1, there are two kinds of nodes in the network: anchors and radars. The anchors are nodes with known positions, while the positions of radars need to be estimated. Anchors and radars can obtain TOA measurements by receiving line-of-sight (LOS) signals. At the same time, considering that radars can receive and transmit signals, we have introduced spatial cooperation between radars to assist in positioning radars in those scenarios where the number of anchors is limited.

### 2.2. Target Sensing Network

The target sensing network model is shown in Figure 2. There are three kinds of nodes in the network—anchors, radars, and targets—where the targets' positions need to be estimated. Anchors and radars can obtain TSOA measurements by receiving non-line-of-sight (NLOS) signals reflected by the targets.

### 2.3. Single-Slot Static ISAL Network

Figure 3 introduces the single-slot static ISAL network. In this network, localization and sensing are simultaneously considered, corresponding to the existence of both the localization transmission links and the sensing transmission links. Only the positions of anchors are known, while the positions of the other two kinds of nodes both need to be estimated. The signal propagation is as follows:

- LOS transmissions between anchors and radars: the anchors and radars send ranging signals to each other to position the radars with active localization. (Localization)
- LOS transmissions between radars themselves: the radars also send ranging signals to the other radars to help the active localization process with the spatial cooperative information contained. (Spatial cooperation for localization)
- NLOS transmissions via the passive targets: the anchors and radars, called active nodes, send sensing signals, which are reflected by the targets, and then received by the other active nodes. (Sensing)

### 2.4. Dual-Slot Dynamic ISAL Network

Figure 4 shows the system model of the dual-slot dynamic ISAL network. In this network, radars and targets are both considered movable, while only the positions of anchors remain the same in different time slots. The signal propagation in each time slot

is the same as that of the single-slot static ISAL network. The major difference is that the radar mobility brings the possibility of introducing temporal cooperation between different time slots based on velocity information obtained from the intra-node measurements, such as Doppler measurements [14]. The temporal cooperation between different time slots can deliver the spatial localization information in the time dimension.

The set of anchors, radars, and targets is respectively represented as  $\mathcal{N}_a = \{1, 2, \dots, N_a\}$ ,  $\mathcal{N}_r = \{1, 2, \dots, N_r\}$ , and  $\mathcal{N}_t = \{1, 2, \dots, N_t\}$ . Here, we only take into consideration that  $N_t = 1$ . The node position is expressed as  $\mathbf{p}_k = [x_k, y_k]^T$ ,  $k \in \mathcal{N}_a \cup \mathcal{N}_r \cup \mathcal{N}_t$ . The distance between different nodes  $i$  and  $j$  is

$$d_{ij} = \|\mathbf{p}_i - \mathbf{p}_j\| = \sqrt{(x_i - x_j)^2 + (y_i - y_j)^2}, \quad (1)$$

and the angle between different nodes  $i$  and  $j$  is

$$\phi_{ij} = \arctan\left(\frac{y_j - y_i}{x_j - x_i}\right). \quad (2)$$

There are two kinds of networks to be discussed, namely, the synchronous and the asynchronous ones. In this article, we mainly discuss the asynchronous networks in which there are only clock offsets between the anchors and different radars, but no clock offsets between anchors. We first consider the two kinds of networks in which one-way ranging (OWR) [27] is used for range estimation. Then, we provide a new ranging strategy called reverse-link-modified one-way ranging (RLM-OWR) to introduce temporal cooperation between the two time slots in the estimation of clock offsets.

In synchronous network, without considering multi-path propagation, the localization signal received by the  $j$ th active node from the  $i$ th active node can be expressed as

$$r_{i,j}(t) = \alpha_{i,j}s_{i,j}(t - \Delta t_{i,j}) + e_{i,j}(t), \quad (3)$$

where  $\alpha_{i,j}$  and  $\Delta t_{i,j}$  are, respectively, the channel gain and the delay of the LOS path from the  $i$ th to the  $j$ th active node, and  $s_{i,j}(t)$  and  $e_{i,j}(t)$ , respectively, represent the transmitted localization signal and the measurement error on the link.

In a synchronous network, the sensing signal transmitted by the  $i$ th active node, received by the  $j$ th active node, and reflected by the target  $tar$  can be expressed as

$$r_{i,tar,j}(t) = \alpha_{i,tar,j}s_{i,tar,j}(t - \Delta t_{i,tar,j}) + e_{i,tar,j}(t), \quad (4)$$

where  $\alpha_{i,tar,j}$  and  $\Delta t_{i,tar,j}$  are, respectively, the channel gain and the delay of the NLOS path from the  $i$ th active node via the target  $tar$  to the  $j$ th active node, and  $s_{i,tar,j}(t)$  and  $e_{i,tar,j}(t)$ , respectively, represent the transmitted sensing signal and the measurement error on the link.

In an asynchronous network, without considering multi-path propagation, the localization signal received by the  $j$ th active node from the  $i$ th active node can be expressed as

$$u_{i,j}(t) = \alpha_{i,j}s_{i,j}(t - \tau_{i,j} - \Delta t_{i,j}) + e_{i,j}(t), \quad (5)$$

where  $\alpha_{i,j}$ ,  $\tau_{i,j}$ , and  $\Delta t_{i,j}$  are, respectively, the channel gain, the clock offset between active node  $i$  and  $j$ , and the delay of the LOS path from the  $i$ th active node to the  $j$ th active node, while  $s_{i,j}(t)$  and  $e_{i,j}(t)$ , respectively, represent the transmitted localization signal and the measurement error on the link.

In an asynchronous network, the sensing signal transmitted by the  $i$ th active node, received by the  $j$ th active node, and reflected by the target  $tar$  can be expressed as

$$u_{i,tar,j}(t) = \alpha_{i,tar,j}s_{i,tar,j}(t - \tau_{i,j} - \Delta t_{i,tar,j}) + e_{i,tar,j}(t), \quad (6)$$

where  $\alpha_{i,tar,j}$ ,  $\tau_{i,j}$ , and  $\Delta t_{i,tar,j}$  are, respectively, the channel gain, the clock offset between active node  $i$  and  $j$ , and the delay of the NLOS path from the  $i$ th active node via the target  $tar$  to the  $j$ th active node, while  $s_{i,tar,j}(t)$  and  $e_{i,tar,j}(t)$ , respectively, represent the transmitted sensing signal and the measurement error on the link.

RLM-OWR is a ranging method that uses OWR for ranging and calibrates the signal propagation delay with the signals on the reverse link. This method can accurately obtain the relative clock drift rates between different clocks in the asynchronous ISAL networks. The schematic diagram is shown in Figures 5 and 6:

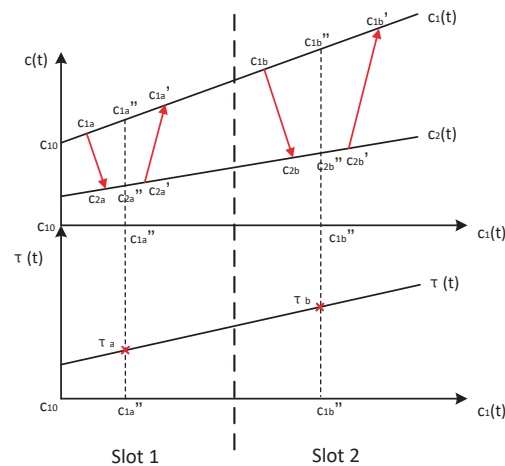


**Figure 5.** RLM-OWR schematic diagram, where the red line represents the signal propagation between two active nodes.

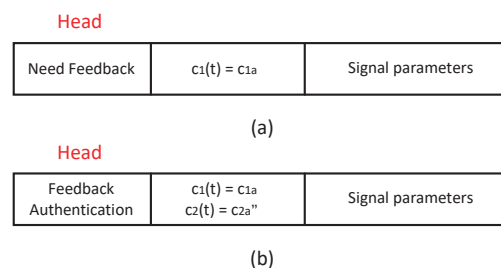


**Figure 6.** RLM-OWR signal packet. (a) Forward link packet. (b) Reverse link packet.

The specific realization of RLM-OWR is as follows:

- (1) Taking the circumstance in slot 1 in Figure 5 as an example, set the clock of node 1  $c_1(t)$  as the reference clock, record  $c_{1a}$  when  $c_1(t) = c_{1a}$ , and broadcast signals with a “Need Feedback” time stamp, which is shown as Figure 6a, to the environment by node 1.
- (2) When the clock of node 2  $c_2(t) = c_{2a}$ , node 2 receives the LOS signal with a “Need Feedback” time stamp transmitted from node 1. After the reply time to  $c_2(t) = c'_{2a}$ , node 2 calculates and records the average of  $c_{2a}$  and  $c'_{2a}$  as  $c''_{2a}$  and transmits the received signal data packet back to node 1 after unloading its head “Need Feedback” and adding another head “Feedback Authentication”. The signal data packet transmitting to node 1 is shown in Figure 6b.
- (3) When the clock of node 1  $c_1(t) = c'_{1a}$ , node 1 receives the LOS signal with a “Feedback Authentication” time stamp transmitted from node 2, and node 1 records its time  $c'_{1a}$ . As the time taken to process the signal data packet in (2) is generally on the microsecond scale, it can be approximately assumed that the positions of the moving nodes remain unchanged during this period. Therefore, we take  $c''_{1a} = \frac{c_{1a} + c'_{1a}}{2}$ , and there is  $c_2(c''_{1a}) = c''_{2a}$ .
- (4) We can obtain  $\tau(c''_{1a}) = \tau_a = c''_{1a} - c''_{2a}$ .



- (5) Similarly, in slot 2, record  $c_{1b}$ ,  $c'_{1b}$ , and  $c''_{2b}$ . We take  $c''_{1b} = \frac{c_{1b} + c'_{1b}}{2}$ , and we can obtain  $\tau(c''_{1b}) = \tau_b = c''_{1b} - c''_{2b}$ .
- (6) According to  $\tau_a$  and  $\tau_b$ , we can obtain the slope of the line  $\tau(t) - t$  in Figure 5, which is known as the relative clock drift rate  $k_\tau = \frac{\Delta\tau(t)}{\Delta t} = \frac{\tau_b - \tau_a}{c''_{1b} - c''_{1a}}$ .

### 3. Fundamental Limits

In this section, we derive the fundamental limits for synchronous and asynchronous ISAL networks, respectively. According to Equations (3)–(6), both localization and sensing can be considered parameter estimation problems. The parameters to be estimated in the  $n$ th time slot of the synchronous ISAL network can be written as

$$\theta^{(n)} = [\mathbf{p}_r^{(n)T}, \mathbf{p}_t^{(n)T}]^T, \quad (7)$$

where  $\mathbf{p}_r^{(n)}$  and  $\mathbf{p}_t^{(n)}$  are the position vectors of radars and targets in the  $n$ th time slot, respectively.

The parameters to be estimated in the  $n$ th time slot of the asynchronous ISAL network can be written as

$$\theta^{(n)} = [\mathbf{p}_r^{(n)T}, \tau^{(n)T}, \mathbf{p}_t^{(n)T}]^T, \quad (8)$$

where  $\mathbf{p}_r^{(n)}$ ,  $\mathbf{p}_t^{(n)}$ , and  $\tau^{(n)}$  are the position vectors of radars and targets and the time offsets between the anchors and different radars in the  $n$ th time slot, respectively.

According to [16], CRLB is often used as the lower bound of the variance of an unbiased estimator. In the ISAL networks, we introduce the squared position error bound (SPEB) instead of CRLB as the lower bound of the mean square error (MSE), which is defined as

$$\mathcal{P}(\theta_1) \triangleq \text{tr}(\mathbf{J}_e^{-1}(\theta_1)) \leq \mathbb{E}(\|\theta_1 - \hat{\theta}_1\|^2), \quad (9)$$

where  $\theta_1$  and  $\hat{\theta}_1$ , respectively, represent one of the parameters in  $\theta$  and an estimate of the parameter vector  $\theta_1$  based on an observation of the received signals, and  $\mathbf{J}_e(\theta_1)$  represents the EFIM of the parameter  $\theta_1$  [17].

#### 3.1. FIM of Synchronous Networks

For a single target ( $N_t = 1$ ) synchronous ISAL network applying the OWR method, another parameter vector that satisfies a mapping with the parameters  $\theta = [\mathbf{p}_r^T, \mathbf{p}_t^T]^T$  is defined as

$$\gamma = [\tau_{1,1}^{\text{sen}}, \dots, \tau_{N_r+N_a, N_r+N_a}^{\text{sen}}, \tau_{1,2}^{\text{ran}}, \dots, \tau_{N_r+N_a, N_r}^{\text{ran}}]^T, \quad (10)$$

where  $\tau_{m,n}^{\text{sen}} = \frac{d_{m,tar} + d_{tar,n}}{c}$ ,  $m, n \in \{m, n | m, n \in \mathcal{N}_r \cup \mathcal{N}_a\}$ ,  $\tau_{m,n}^{\text{ran}} = \frac{d_{m,n}}{c}$ ,  $m, n \in \{m, n | m \in \mathcal{N}_r, n \in \mathcal{N}_r \cup \mathcal{N}_a, m \neq n\} \cup \{m, n | m \in \mathcal{N}_a, n \in \mathcal{N}_r\}$ .

Assuming that the received signals  $\mathbf{r} = [r_{1,1}^{\text{sen}}, \dots, r_{N_r+N_a, N_r+N_a}^{\text{sen}}, r_{1,2}^{\text{ran}}, \dots, r_{N_r+N_a, N_r}^{\text{ran}}]^T$ , due to the independence of the received signals corresponding to different links, according to the definition of FIM, the conditional probability density function  $f(\mathbf{r}|\gamma)$  is

$$f(\mathbf{r}|\gamma) = \prod_{m,n \in \mathcal{N}_r \cup \mathcal{N}_a} f(r_{m,n}^{\text{sen}}|\gamma) \prod_{m,n \in \{m,n | m \in \mathcal{N}_r, n \in \mathcal{N}_r \cup \mathcal{N}_a, m \neq n\} \cup \{m,n | m \in \mathcal{N}_a, n \in \mathcal{N}_r\}} f(r_{m,n}^{\text{ran}}|\gamma), \quad (11)$$

the FIM for the parameter vector  $\gamma$  is

$$\mathbf{I}_\gamma = \mathbb{E}_{\mathbf{r}|\gamma} \left\{ \left[ \frac{\partial \ln f(\mathbf{r}|\gamma)}{\partial \gamma} \right] \left[ \frac{\partial \ln f(\mathbf{r}|\gamma)}{\partial \gamma} \right]^T \right\}, \quad (12)$$

and after some derivation,  $\mathbf{I}_\gamma$  can be written as

$$\mathbf{I}_\gamma = c^2 \times \begin{bmatrix} \lambda_{1,tar,1} & \cdots & 0 \\ \vdots & \ddots & \vdots \\ 0 & \cdots & \lambda_{N_r+N_a, N_r} \end{bmatrix}, \quad (13)$$



where  $\lambda_{m,n}, m, n \in \{m, n | m \in \mathcal{N}_r, n \in \mathcal{N}_r \cup \mathcal{N}_a, m \neq n\} \cup \{m, n | m \in \mathcal{N}_a, n \in \mathcal{N}_r\}$  and  $\lambda_{m,tar,n}, m, n \in \{m, n | m, n \in \mathcal{N}_r \cup \mathcal{N}_a\}$ , respectively, represent the range information intensity (RII) of the localization and sensing links, which can be expressed as

$$\lambda_{m,n} = \frac{8\pi^2 B^2}{c^2} \frac{P_m G_m G_n c^2}{(4\pi)^2 d_{m,n}^2 N_0 B L f_c^2} = \xi_{m,n} \frac{P_m}{d_{m,n}^2} \quad (14)$$

$$\lambda_{m,tar,n} = \frac{8\pi^2 B^2}{c^2} \frac{P_m G_m G_n c^2}{(4\pi)^2 d_{m,tar}^2 d_{tar,n}^2 N_0 B L f_c^2} \frac{\sigma}{4\pi} = \xi_{m,tar,n} \frac{P_m}{d_{m,tar}^2 d_{tar,n}^2} \frac{\sigma}{4\pi}, \quad (15)$$

where  $m, tar$ , and  $n$ , respectively, represent the  $m$ th transmitting node, the target, and the  $n$ th receiving node;  $B$  is the signal bandwidth;  $c$  is the speed of light;  $P_m$  is the signal transmission power;  $G_m$  and  $G_n$ , respectively, represent the antenna gain of the transmitter and receiver;  $N_0$  is the power spectral density of environmental thermal noise;  $L$  is the communication system loss;  $f_c$  is the carrier frequency of the signal;  $\sigma$  is the radar cross section; and  $\xi_{m,n}$  and  $\xi_{m,tar,n}$  are, respectively, the common constant coefficient in the RII of the localization link and the sensing link.

By means of a bijective transformation [17], the FIM for the parameter vector  $\theta$  can be expressed as

$$\mathbf{I}_\theta = \mathbf{J}^T \mathbf{I}_\gamma \mathbf{J}, \quad (16)$$

where  $\mathbf{J}$  is the Jacobian matrix for the transmission from  $\theta$  to  $\gamma$ , which can be written as

$$\mathbf{J} = \frac{\partial \gamma}{\partial \theta} = \left[ \frac{\partial \gamma}{\partial \mathbf{p}_r}, \frac{\partial \gamma}{\partial \mathbf{p}_t} \right], \quad (17)$$

where the specific expressions of  $\frac{\partial \gamma}{\partial \mathbf{p}_r}$  and  $\frac{\partial \gamma}{\partial \mathbf{p}_t}$  are given in Appendix A.1.

Based on the results above, the FIM expression for the single-slot synchronous ISAL networks can be derived, which can be expressed in the following form:

$$\mathbf{I}_\theta^{\text{syn}} = \begin{bmatrix} \mathbf{J}_e^R & \mathbf{S}_{R,T} \\ \mathbf{S}_{R,T}^T & \mathbf{J}_e^T \end{bmatrix}_{2(N_r+N_t) \times 2(N_r+N_t)}, \quad (18)$$

where  $\mathbf{J}_e^R$ ,  $\mathbf{J}_e^T$ , and  $\mathbf{S}_{R,T}$  are the submatrices in  $\mathbf{I}_\theta^{\text{syn}}$ , with respect to the radar localization information, the target sensing information, and the spatial cooperation information between radar localization and target sensing.

For the FIM of multi-slot synchronous ISAL networks, since we can obtain the velocity information of the moving active nodes, we can predict the positions of the moving active nodes in the next time slot, corresponding to the time cooperation information of radar positioning between time slots in the FIM. Considering the complexity of the multi-slot ISAL networks, we give the expression of the FIM of the dual-slot synchronous ISAL networks as follows [26]:

$$\mathbf{I}_\theta^{\text{syn}(2)} = \begin{bmatrix} \mathbf{J}_e^{R(1)} + \mathbf{T}_{\text{Loc}}^{(1)} & \mathbf{S}_{R,T}^{(1)} & \mathbf{T}_{\text{Loc}}^{(1)} & \mathbf{0} \\ \mathbf{S}_{R,T}^{(1)T} & \mathbf{J}_e^{T(1)} & \mathbf{0} & \mathbf{0} \\ \mathbf{T}_{\text{Loc}}^{(1)} & \mathbf{0} & \mathbf{J}_e^{R(2)} + \mathbf{T}_{\text{Loc}}^{(1)} & \mathbf{S}_{R,T}^{(2)} \\ \mathbf{0} & \mathbf{0} & \mathbf{S}_{R,T}^{(2)T} & \mathbf{J}_e^{T(2)} \end{bmatrix}, \quad (19)$$

where superscript  $(n)$ ,  $n = 1, 2$  represents the  $n$ th time slot, and submatrix  $\mathbf{T}_{\text{Loc}}$  contains the temporal cooperation information on radar positioning [14], which is expressed as

$$\mathbf{T}_{\text{Loc}} = \begin{bmatrix} \frac{1}{\eta^2} & 0 & \cdots & 0 \\ 0 & \frac{1}{\eta^2} & \cdots & 0 \\ \vdots & \vdots & \ddots & \vdots \\ 0 & 0 & \cdots & \frac{1}{\eta^2} \end{bmatrix}_{2N_r \times 2N_r}, \quad (20)$$

where  $\eta^2$  is the variance of node velocity.

### 3.2. FIM of Asynchronous Networks

For a single target ( $N_t = 1$ ) asynchronous ISAL network applying the OWR method, another parameter vector that satisfies a mapping with the parameters  $\boldsymbol{\theta} = [\mathbf{p}_r^T, \boldsymbol{\tau}^T, \mathbf{p}_t^T]^T$  is defined as

$$\boldsymbol{\zeta} = [v_{1,1}^{\text{sen}}, \dots, v_{N_r+N_a, N_r+N_a}^{\text{sen}}, v_{1,2}^{\text{ran}}, \dots, v_{N_r+N_a, N_r}^{\text{ran}}]^T, \quad (21)$$

where  $v_{m,n}^{\text{sen}} = \frac{d_{m,\text{tar}} + d_{\text{tar},n}}{c} + \tau_{m,n}$ ,  $m, n \in \{m, n | m, n \in \mathcal{N}_r \cup \mathcal{N}_a\}$ ,  $v_{m,n}^{\text{ran}} = \frac{d_{m,n}}{c} + \tau_{m,n}$ ,  $m, n \in \{m, n | m \in \mathcal{N}_r, n \in \mathcal{N}_r \cup \mathcal{N}_a, m \neq n\} \cup \{m, n | m \in \mathcal{N}_a, n \in \mathcal{N}_r\}$ .

Similar to the synchronous ISAL networks, we can obtain the FIM of  $\boldsymbol{\zeta}$  expressed as (13), and the FIM of  $\boldsymbol{\theta}$  can also be obtained from (16).

The Jacobian matrix for the transformation from  $\boldsymbol{\theta}$  to  $\boldsymbol{\zeta}$  in the asynchronous ISAL network can be expressed as

$$\mathbf{J} = \frac{\partial \boldsymbol{\zeta}}{\partial \boldsymbol{\theta}} = \left[ \frac{\partial \boldsymbol{\zeta}}{\partial \mathbf{p}_r}, \frac{\partial \boldsymbol{\zeta}}{\partial \boldsymbol{\tau}}, \frac{\partial \boldsymbol{\zeta}}{\partial \mathbf{p}_t} \right], \quad (22)$$

where the specific expressions of  $\frac{\partial \boldsymbol{\zeta}}{\partial \mathbf{p}_r}$ ,  $\frac{\partial \boldsymbol{\zeta}}{\partial \boldsymbol{\tau}}$ , and  $\frac{\partial \boldsymbol{\zeta}}{\partial \mathbf{p}_t}$  are given in Appendix A.2.

Based on the results above, the FIM expression of the single-slot asynchronous ISAL networks can be derived, which can be expressed in the following form:

$$\mathbf{I}_{\boldsymbol{\theta}}^{\text{asyn}} = \begin{bmatrix} \mathbf{J}_e^R & \mathbf{S}_{R,\tau} & \mathbf{S}_{R,T} \\ \mathbf{S}_{R,\tau}^T & \mathbf{J}_e^\tau & \mathbf{S}_{T,\tau} \\ \mathbf{S}_{R,T}^T & \mathbf{S}_{T,\tau}^T & \mathbf{J}_e^T \end{bmatrix}_{[2(N_r+N_t)+|\mathcal{N}_r|] \times [2(N_r+N_t)+|\mathcal{N}_r|]}, \quad (23)$$

where  $\mathbf{J}_e^T$ ,  $\mathbf{S}_{R,\tau}$ , and  $\mathbf{S}_{T,\tau}$  are the submatrices in  $\mathbf{I}_{\boldsymbol{\theta}}^{\text{asyn}}$  with respect to the clock offset information, the cooperation information between radar localization and clock offset, and the cooperation information between target sensing and clock offset.

According to the principle of RLM-OWR, for the FIM of multi-slot asynchronous ISAL networks, in addition to introducing radar positioning temporal cooperation information between time slots through Doppler measurement, we can also obtain the relative clock drift rate through RLM-OWR, thereby further introducing temporal cooperation information for estimating clock offsets between time slots. Considering the complexity of the multi-slot ISAL networks, here we give the expression of the FIM of the dual-slot asynchronous ISAL networks after applying RLM-OWR, which is shown as (24)

$$\mathbf{I}_{\boldsymbol{\theta}}^{\text{asyn}(2)} = \begin{bmatrix} \mathbf{J}_e^{R(1)} + \mathbf{T}_{\text{Loc}}^{(1)} & \mathbf{S}_{R,\tau}^{(1)} & \mathbf{S}_{R,T}^{(1)} & \mathbf{T}_{\text{Loc}}^{(1)} & \mathbf{0} & \mathbf{0} \\ \mathbf{S}_{R,\tau}^{(1)T} & \mathbf{J}_e^{\tau(1)} + \mathbf{T}_\tau^{(1)} & \mathbf{S}_{T,\tau}^{(1)} & \mathbf{0} & \mathbf{T}_\tau^{(1)} & \mathbf{0} \\ \mathbf{S}_{R,T}^{(1)T} & \mathbf{S}_{T,\tau}^{(1)T} & \mathbf{J}_e^{T(1)} & \mathbf{0} & \mathbf{0} & \mathbf{0} \\ \mathbf{T}_{\text{Loc}}^{(1)} & \mathbf{0} & \mathbf{0} & \mathbf{J}_e^{R(2)} + \mathbf{T}_{\text{Loc}}^{(1)} & \mathbf{S}_{R,\tau}^{(2)} & \mathbf{S}_{R,T}^{(2)} \\ \mathbf{0} & \mathbf{T}_\tau^{(1)} & \mathbf{0} & \mathbf{S}_{R,\tau}^{(2)T} & \mathbf{J}_e^{\tau(2)} + \mathbf{T}_\tau^{(1)} & \mathbf{S}_{T,\tau}^{(2)} \\ \mathbf{0} & \mathbf{0} & \mathbf{0} & \mathbf{S}_{R,T}^{(2)T} & \mathbf{S}_{T,\tau}^{(2)T} & \mathbf{J}_e^{T(2)} \end{bmatrix}, \quad (24)$$

where submatrix  $\mathbf{T}_\tau$  contains the temporal cooperation information on the clock offset, which is expressed as

$$\mathbf{T}_\tau = \begin{bmatrix} \frac{1}{\rho^2} & 0 & \cdots & 0 \\ 0 & \frac{1}{\rho^2} & \cdots & 0 \\ \vdots & \vdots & \ddots & \vdots \\ 0 & 0 & \cdots & \frac{1}{\rho^2} \end{bmatrix}_{|\mathcal{N}_r| \times |\mathcal{N}_r|}, \quad (25)$$

where  $\rho^2$  is the variance of relative clock drift rate.

#### 4. Energy and Power Optimization Allocation

In practical ISAL networks, network resources such as energy and bandwidth are often constrained. Therefore, in order to improve the accuracy of localization and sensing as much as possible, it is necessary to optimize the allocation of network resources. In this section, we mainly discuss the optimal allocation of power in the single-slot ISAL networks, as well as the optimal allocation of energy between time slots in the multi-slot ISAL networks. We propose two resource optimization schemes—a step-by-step scheme and an integrated scheme—and summarize the suitable scenarios for each of them.

Firstly, we introduce the meanings of the step-by-step and the integrated scheme, respectively. For an ISAL network, assuming that the parameters are  $\theta = [\theta_1^T, \dots, \theta_N^T]^T$ , in the integrated optimization scheme, we simultaneously optimize and allocate resources to all of the  $N$  variables in  $\theta$ ; in the step-by-step optimization scheme, we only optimize and allocate resources to one single variable in  $\theta$  and apply the resource optimization allocation result of the previous variable as prior knowledge to the optimization of the next variable. This converts the multi-variable optimization problem into multiple single-variable optimization problems and solves them step-by-step, which can avoid the optimization difficulties caused by dealing with multiple variables; however, it also comes at a cost of high time complexity.

Based on the statement above, we need to minimize the time complexity of the step-by-step scheme when dealing with multi-variable optimization problems such as those in ISAL networks. In addition to designing optimization algorithms with low time complexity, this article explores the resource allocation of ISAL networks with different topologies and finds the regularity of energy allocation for step-by-step optimization schemes in the networks. This provides some theoretical reference value for practical step-by-step optimization schemes in ISAL networks. In addition, this article also analyzes the energy allocation between time slots in the dual-slot ISAL networks.

##### 4.1. Integrated Optimization Scheme

###### 4.1.1. Optimization for Synchronous Networks

For the single-slot synchronous ISAL network, the FIM of  $\theta = [\mathbf{p}_r^T, \mathbf{p}_t^T]^T$  is as in (18), and the power optimization allocation strategy is as in [25]:

$$\mathfrak{B}_1: \min \quad \text{tr}(\mathbf{J}_e^{\text{T}-1}) \quad (26)$$

$$\text{s.t.} \quad \sum_{j \in \mathcal{N}_a \cup \mathcal{N}_r} P_j \leq E_{\text{total}}/1 \quad (27)$$

$$0 \leq P_j \leq P_{r,\max}, \forall j \in \mathcal{N}_r \quad (28)$$

$$0 \leq P_j \leq P_{a,\max}, \forall j \in \mathcal{N}_a, \quad (29)$$

where  $E_{\text{total}}$  is the total energy of the ISAL network, and  $P_{a,\max}$  and  $P_{r,\max}$  are the upper limit of power allocated to each anchor and radar, respectively, within a single slot.

According to [24], problem  $\mathfrak{B}_1$  can be reformulated into a standard semi-definite programming (SDP) problem as:

$$\mathfrak{A}_1^{\text{SDP}} : \min \text{tr}(\mathbf{H})_{\mathbf{p}_t} \quad (30)$$

$$\text{s.t. } \mathbf{H} \succeq 0 \quad (31)$$

$$\begin{bmatrix} \mathbf{H} & \mathbf{I} \\ \mathbf{I} & \mathbf{I}_{\theta}^{\text{syn}} \end{bmatrix} \succeq 0 \quad (32)$$

$$\sum_{j \in \mathcal{N}_a \cup \mathcal{N}_r} P_j \leq E_{\text{total}}/1 \quad (33)$$

$$0 \leq P_j \leq P_{r,\max}, \forall j \in \mathcal{N}_r \quad (34)$$

$$0 \leq P_j \leq P_{a,\max}, \forall j \in \mathcal{N}_a, \quad (35)$$

where  $\mathbf{H}$  is called the auxiliary matrix of the FIM, and  $\mathbf{I}$  represents the identity matrix whose dimension is the same as the FIM.

For the dual-slot synchronous ISAL network, the FIM expression is as in (19). We search for the optimal energy allocation between two time slots through traversal, where the energy allocated to slot 1 and slot 2 is, respectively,  $E_{\text{slot1}}$  and  $E_{\text{slot2}}$ , satisfying  $E_{\text{total}} = E_{\text{slot1}} + E_{\text{slot2}}$ . The power optimization allocation strategy within slot 1 is the same as that in the single-slot synchronous ISAL networks. The power optimization allocation within slot 2 applies the result in slot 1 as prior knowledge, which is shown as

$$\mathfrak{A}_2^{\text{SDP}} : \min \text{tr}(\mathbf{H})_{\mathbf{p}_t^{(2)}} \quad (36)$$

$$\text{s.t. } \mathbf{H} \succeq 0 \quad (37)$$

$$\begin{bmatrix} \mathbf{H} & \mathbf{I} \\ \mathbf{I} & \mathbf{I}_{\theta}^{\text{syn}(2)} \end{bmatrix} \succeq 0 \quad (38)$$

$$\sum_{j \in \mathcal{N}_a \cup \mathcal{N}_r} P_j \leq E_{\text{slot2}}/1 \quad (39)$$

$$0 \leq P_j \leq P_{r,\max}, \forall j \in \mathcal{N}_r \quad (40)$$

$$0 \leq P_j \leq P_{a,\max}, \forall j \in \mathcal{N}_a. \quad (41)$$

#### 4.1.2. Optimization for Asynchronous Networks

For the single-slot asynchronous ISAL network, the FIM of  $\theta = [\mathbf{p}_r^T, \tau^T, \mathbf{p}_t^T]^T$  is as in (23), and the power optimization allocation strategy is as follows:

$$\mathfrak{A}_3^{\text{SDP}} : \min \text{tr}(\mathbf{H})_{\mathbf{p}_t} \quad (42)$$

$$\text{s.t. } \mathbf{H} \succeq 0 \quad (43)$$

$$\begin{bmatrix} \mathbf{H} & \mathbf{I} \\ \mathbf{I} & \mathbf{I}_{\theta}^{\text{asyn}} \end{bmatrix} \succeq 0 \quad (44)$$

$$\sum_{j \in \mathcal{N}_a \cup \mathcal{N}_r} P_j \leq E_{\text{total}}/1 \quad (45)$$

$$0 \leq P_j \leq P_{r,\max}, \forall j \in \mathcal{N}_r \quad (46)$$

$$0 \leq P_j \leq P_{a,\max}, \forall j \in \mathcal{N}_a. \quad (47)$$

For the dual-slot asynchronous ISAL network, the FIM is expressed as in (24). Similar to the synchronous network, we search for the optimal energy allocation between two time slots through traversal. The power optimization allocation strategy within slot 1 is the

same as that of the single-slot asynchronous network. The power optimization allocation within slot 2 applies the result in slot 1 as prior knowledge, which is shown as follows:

$$\mathfrak{A}_4^{\text{SDP}} : \min \text{tr}(\mathbf{H})_{\mathbf{p}_t^{(2)}} \quad (48)$$

$$\text{s.t. } \mathbf{H} \succeq 0 \quad (49)$$

$$\begin{bmatrix} \mathbf{H} & \mathbf{I} \\ \mathbf{I} & \mathbf{I}_{\theta}^{\text{asyn}(2)} \end{bmatrix} \succeq 0 \quad (50)$$

$$\sum_{j \in \mathcal{N}_a \cup \mathcal{N}_r} P_j \leq E_{\text{slot2}}/1 \quad (51)$$

$$0 \leq P_j \leq P_{r,\max}, \forall j \in \mathcal{N}_r \quad (52)$$

$$0 \leq P_j \leq P_{a,\max}, \forall j \in \mathcal{N}_a. \quad (53)$$

#### 4.2. Step-by-Step Optimization Scheme

In the step-by-step optimization scheme, each optimization step only focuses on a single parameter vector, and the optimization results of the previous step can serve as prior knowledge for subsequent steps. Here, we only give the power optimization allocation strategy for the single-slot synchronous and asynchronous ISAL networks. According to the optimization allocation method in the single-slot networks, the power optimization allocation in the dual-slot networks is easy to obtain.

##### 4.2.1. Optimization for Synchronous Networks

For the single-slot synchronous ISAL network, there are two steps in the step-by-step scheme, and the power optimization allocation strategy is as follows:

Step 1 : Radar Localization

$$\mathfrak{A}_5^{\text{SDP}} : \min \text{tr}(\mathbf{H}_r)_{\mathbf{p}_r} \quad (54)$$

$$\text{s.t. } \mathbf{H}_r \succeq 0 \quad (55)$$

$$\begin{bmatrix} \mathbf{H}_r & \mathbf{I} \\ \mathbf{I} & \mathbf{J}_e^R \end{bmatrix} \succeq 0 \quad (56)$$

$$\sum_{j \in \mathcal{N}_a \cup \mathcal{N}_r} P_j \leq E_{\text{step1}}/1 \quad (57)$$

$$0 \leq P_j \leq P_{r,\max}, \forall j \in \mathcal{N}_r \quad (58)$$

$$0 \leq P_j \leq P_{a,\max}, \forall j \in \mathcal{N}_a; \quad (59)$$

Step 2: Target Sensing

$$\mathfrak{A}_6^{\text{SDP}} : \min \text{tr}(\mathbf{H}_{r,t})_{\mathbf{p}_t} \quad (60)$$

$$\text{s.t. } \mathbf{H}_{r,t} \succeq 0 \quad (61)$$

$$\begin{bmatrix} \mathbf{H}_{r,t} & \mathbf{I} \\ \mathbf{I} & \mathbf{I}_{\theta}^{\text{syn}} \end{bmatrix} \succeq 0 \quad (62)$$

$$\sum_{j \in \mathcal{N}_a \cup \mathcal{N}_r} P_j \leq E_{\text{step2}}/1 \quad (63)$$

$$0 \leq P_j \leq P_{r,\max}, \forall j \in \mathcal{N}_r \quad (64)$$

$$0 \leq P_j \leq P_{a,\max}, \forall j \in \mathcal{N}_a, \quad (65)$$

where  $\mathbf{H}_r$  and  $\mathbf{H}_{r,t}$  are the auxiliary matrices, the total energy  $E_{\text{total}} = E_{\text{step1}} + E_{\text{step2}}$ , and there is prior knowledge of  $\mathbf{J}_e^R$  obtained from step 1 in  $\mathbf{I}_{\theta}^{\text{syn}}$  in (62).

#### 4.2.2. Optimization for Asynchronous Networks

For the single-slot asynchronous ISAL network, there are three steps in the step-by-step scheme, and the power optimization allocation strategy is as follows:

Step 1: Radar Localization

$$\mathfrak{A}_7^{\text{SDP}} : \min \text{tr}(\mathbf{H}_r)_{\mathbf{p}_r} \quad (66)$$

$$\text{s.t. } \mathbf{H}_r \succeq 0 \quad (67)$$

$$\begin{bmatrix} \mathbf{H}_r & \mathbf{I} \\ \mathbf{I} & \mathbf{J}_e^R \end{bmatrix} \succeq 0 \quad (68)$$

$$\sum_{j \in \mathcal{N}_a \cup \mathcal{N}_r} P_j \leq E_{\text{step1}}/1 \quad (69)$$

$$0 \leq P_j \leq P_{r,\max}, \forall j \in \mathcal{N}_r \quad (70)$$

$$0 \leq P_j \leq P_{a,\max}, \forall j \in \mathcal{N}_a; \quad (71)$$

Step 2: Clock Offset Estimation

$$\mathfrak{A}_8^{\text{SDP}} : \min \text{tr}(\mathbf{H}_{r,\tau})_{\tau} \quad (72)$$

$$\text{s.t. } \mathbf{H}_{r,\tau} \succeq 0 \quad (73)$$

$$\begin{bmatrix} \mathbf{H}_{r,\tau} & \mathbf{I} \\ \mathbf{I} & \mathbf{J}_{\text{sub}} \end{bmatrix} \succeq 0 \quad (74)$$

$$\sum_{j \in \mathcal{N}_a \cup \mathcal{N}_r} P_j \leq E_{\text{step2}}/1 \quad (75)$$

$$0 \leq P_j \leq P_{r,\max}, \forall j \in \mathcal{N}_r \quad (76)$$

$$0 \leq P_j \leq P_{a,\max}, \forall j \in \mathcal{N}_a; \quad (77)$$

Step 3: Target Sensing

$$\mathfrak{A}_9^{\text{SDP}} : \min \text{tr}(\mathbf{H}_{r,\tau,t})_{\mathbf{p}_t} \quad (78)$$

$$\text{s.t. } \mathbf{H}_{r,\tau,t} \succeq 0 \quad (79)$$

$$\begin{bmatrix} \mathbf{H}_{r,\tau,t} & \mathbf{I} \\ \mathbf{I} & \mathbf{I}_{\theta}^{\text{asyn}} \end{bmatrix} \succeq 0 \quad (80)$$

$$\sum_{j \in \mathcal{N}_a \cup \mathcal{N}_r} P_j \leq E_{\text{step3}}/1 \quad (81)$$

$$0 \leq P_j \leq P_{r,\max}, \forall j \in \mathcal{N}_r \quad (82)$$

$$0 \leq P_j \leq P_{a,\max}, \forall j \in \mathcal{N}_a, \quad (83)$$

where  $\mathbf{H}_r$ ,  $\mathbf{H}_{r,\tau}$ , and  $\mathbf{H}_{r,\tau,t}$  are the auxiliary matrices; the total energy  $E_{\text{total}} = E_{\text{step1}} + E_{\text{step2}} + E_{\text{step3}}$ ;  $\mathbf{J}_{\text{sub}} = (\mathbf{I}_{\theta}^{\text{asyn}})_{1:2N_r+|\mathcal{N}_r|, 1:2N_r+|\mathcal{N}_r|}$ ; and there is prior knowledge of  $\mathbf{J}_e^R$  obtained from step 1 in  $\mathbf{J}_{\text{sub}}$  in (74), as well as a prior knowledge  $\mathbf{J}_{\text{sub}}$  obtained from step 2 in  $\mathbf{I}_{\theta}^{\text{asyn}}$  in (80).

#### 5. Numerical Results and Discussion

From the previous section, it can be seen that the reason the step-by-step scheme has high time complexity is that it searches for the optimal energy allocation scheme through traversal. To compensate for the high time complexity of the step-by-step scheme, this section starts by exploring the optimal energy allocation for each step in a single time slot and for each time slot between multiple time slots. The regular conclusion of energy optimization allocation for the step-by-step scheme is given. By comparing the sensing accuracy of the step-by-step and the integrated scheme in networks with different topologies, a suitable network topology for each of the two schemes is given.

### 5.1. Network Settings

#### 5.1.1. Single-Slot Network Settings

For the single-slot ISAL networks, we present four networks with different topologies in the area of  $200\text{ m} \times 200\text{ m}$ , as shown in Figure 7. The solid red circles represent the anchors, the solid green triangles represent the radars, and the solid black pentagram represents the target. These four networks all contain two anchors, two radars, and one target.

#### 5.1.2. Dual-Slot Network Settings

For the dual-slot ISAL networks, we present four networks with different topologies in the area of  $200\text{ m} \times 200\text{ m}$ , as shown in Figure 8. The solid red circles represent anchors whose positions remain unchanged within two time slots; the solid green triangles and the solid black pentagram, respectively, represent radars and target in slot 1; and the hollow green triangles and the hollow black pentagram, respectively, represent radars and target in slot 2. Within each time slot, all four networks contain two anchors, two radars, and one target.

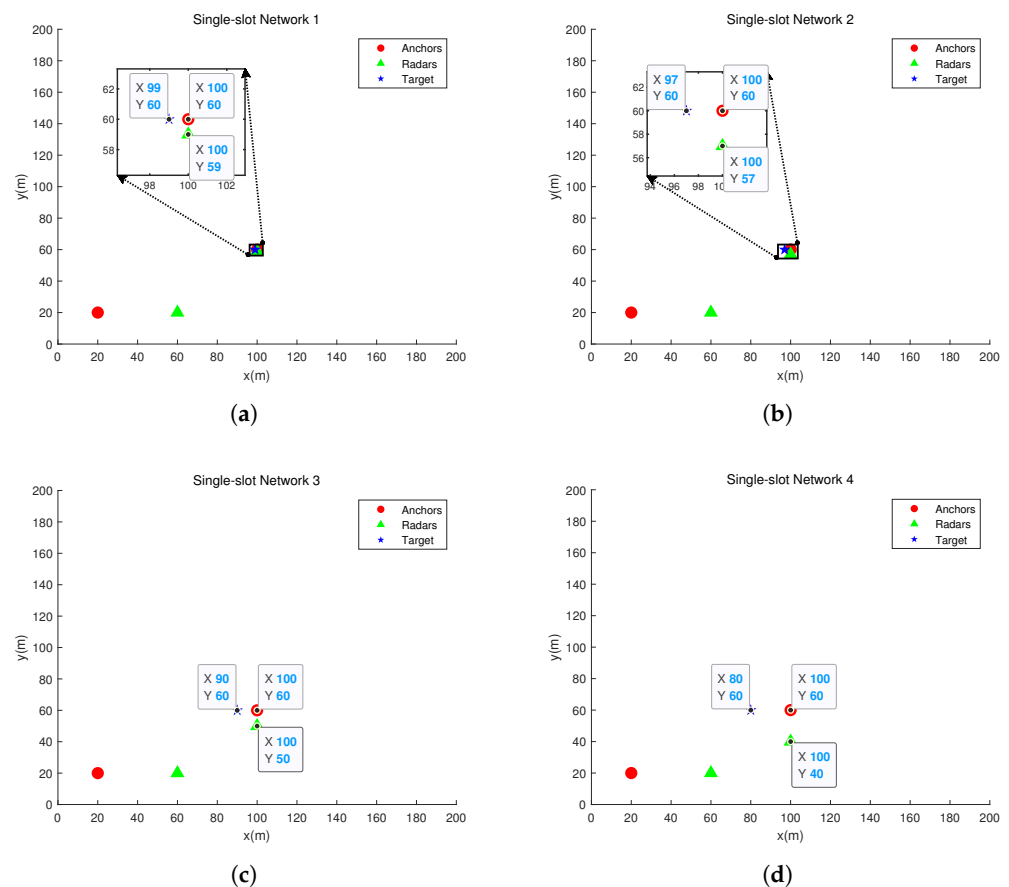


**Figure 7.** Four single-slot networks. (a,b) Sensing-resource-abundant networks. (c,d) Sensing-resource-limited networks.

#### 5.1.3. Simulation Parameters

The relevant parameters in the simulation can be seen in Table 1.



**Table 1.** Simulation parameters.

Parameter	Symbol	Value
Carrier frequency	$f_c$	77 GHz
Total energy	$E_{\text{total}}$	10 J
Total bandwidth	$B_{\text{total}}$	500 MHz
Antenna gain	$G$	10 dB
Noise power spectral density	$N_0$	−174 dBm/Hz
Upper limit of anchor power	$P_{a,\text{max}}$	1
Upper limit of radar power	$P_{r,\text{max}}$	1
Radar cross section	$\sigma$	10 m <sup>2</sup>
System loss	$L$	3 dB
Variance of node velocity	$\eta^2$	0.01 m <sup>2</sup> /s <sup>2</sup>
Variance of relative clock drift rate	$\rho^2$	$1 \times 10^{-10}$

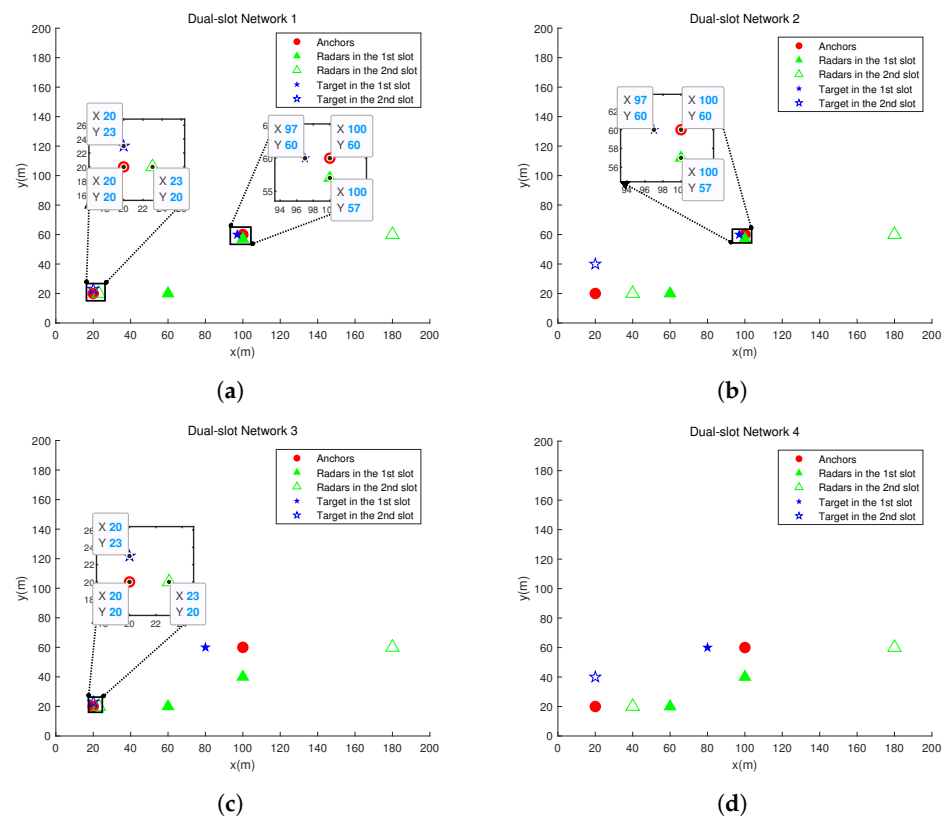


**Figure 8.** Four dual-slot networks. (a) Sensing-resource-abundant networks in both slots. (b) Sensing-resource-abundant network in the first slot and sensing-resource-limited network in the second slot. (c) Sensing-resource-limited network in the first slot and sensing-resource-abundant network in the second slot. (d) Sensing-resource-limited networks in both slots.

## 5.2. Synchronous Networks

### 5.2.1. Single-Slot Networks

For the single-slot synchronous ISAL networks, as shown in Figure 9, we provide a comparison of the sensing SPEB results between the step-by-step and the integrated scheme in the four networks in Figure 7.

Due to the fact that all active nodes in this study can both transmit and receive signals, the target sensing can be achieved by only two active nodes through twice TOA and once TSOA. In Figure 7, we set up a variably-sized partial network with one target and two active nodes. The networks with relatively close distances among three nodes are called

sensing-resource-abundant networks. On the other hand, the networks with relatively far distances among three nodes are called sensing-resource-limited networks.

According to Figure 9, we have the following observations. Firstly, when the distribution of nodes is relatively uniform in the ISAL network, in other words, when the length of the localization and sensing links in the network is basically the same level (such as  $1 \times 10^1 \sim 1 \times 10^2$  m), the step-by-step optimization scheme will allocate the majority of the total energy to the second step for target sensing, as shown in the Figure 9d. This indicates that, in the networks with evenly distributed nodes, the difficulty of sensing passive targets is much higher than the difficulty of locating active nodes. Secondly, in the single-slot synchronous ISAL networks, when optimizing the sensing SPEB, the step-by-step optimization scheme is more suitable for the sensing-resource-abundant networks, as shown in Figure 9a,b. The integrated optimization scheme is more suitable for the sensing-resource-limited networks, as shown in Figure 9c,d. In addition, from the SPEB results of the step-by-step scheme of the single-slot synchronous ISAL networks, we can observe the trade-off relationship between sensing and localization, as shown in Figure 9b,c.

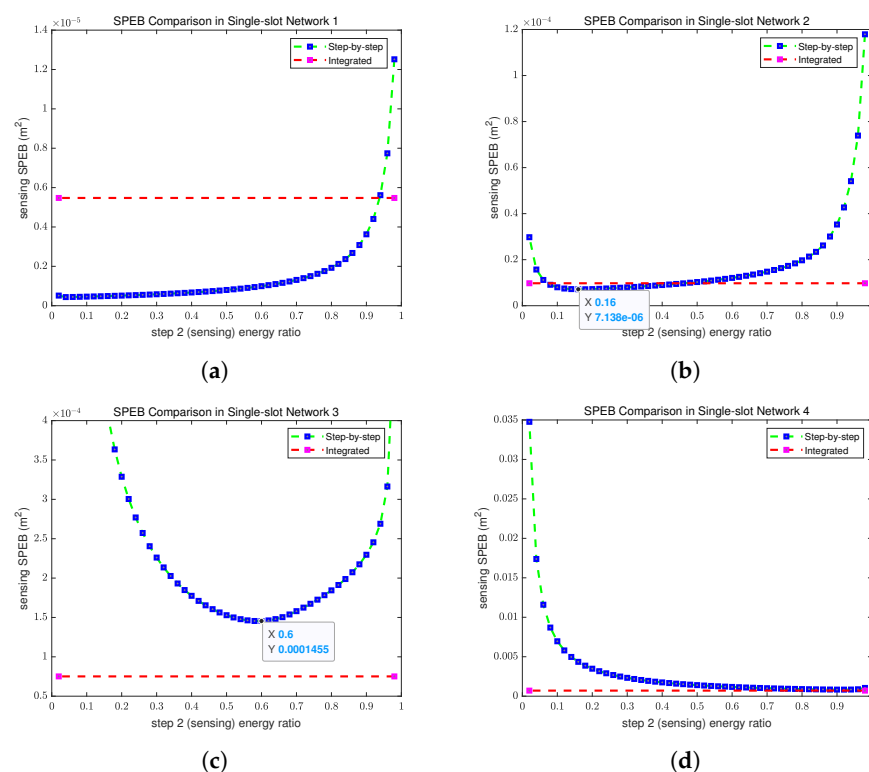


**Figure 9.** SPEB comparison between the step-by-step scheme and the integrated scheme in four single-slot synchronous networks. (a) SPEB comparison in a single-slot synchronous network (Figure 7a). (b) SPEB comparison in a single-slot synchronous network (Figure 7b). (c) SPEB comparison in a single-slot synchronous network (Figure 7c). (d) SPEB comparison in a single-slot synchronous network (Figure 7d).

From the conclusions above, we provide the following interpretations. Firstly, it is not difficult to find that, when the length of the localization and sensing links is basically the same level, the RII of the sensing link is much smaller than that of the localization link. Therefore, when the network nodes are evenly distributed, the difficulty of sensing passive targets is relatively higher. Secondly, in the sensing-resource-abundant networks, target sensing requires less energy than radar positioning. Due to the flexibility of energy allocation between two steps, the step-by-step scheme can reduce the energy allocated for step 2 (target sensing) to allow more energy to be used for radar positioning, which is beneficial for improving radar positioning accuracy. We take the comparison between Figure 9b,c as an example. It is not difficult to find that, based on the inflection points of the SPEB curves in Figure 9b,c, in the sensing-resource-abundant network, 44% of

the total energy is further allocated to step 1 for radar positioning, leading to a smaller sensing SPEB in the step-by-step scheme than in the integrated scheme. Additionally, the optimization results of step 1 (radar positioning) in the step-by-step scheme can serve as prior information for step 2. Therefore, the improvement of radar positioning accuracy has a positive promoting effect on the improvement of target sensing accuracy. However, in the integrated optimization scheme, due to simultaneous radar positioning and target sensing and the optimization of the sensing SPEB, poor radar positioning accuracy will be obtained by the integrated scheme, which is detrimental to the accuracy of target sensing. Therefore, the step-by-step scheme is more suitable for sensing-resource-abundant networks.

For sensing-resource-limited networks, as radar positioning is easier than target sensing, the optimized power allocation results for target sensing in the integrated optimization scheme can meet the needs of radar positioning in the networks. In this situation, the accuracy of radar positioning obtained by the integrated scheme will have no adverse impact on its sensing accuracy. However, in the step-by-step scheme, in order to ensure that the accuracy of radar positioning does not have an adverse impact on sensing accuracy, a portion of energy needs to be allocated to step 1 for radar positioning, resulting in a reduction in the energy allocated to step 2 for target sensing. Due to the fact that target sensing is harder than radar positioning in sensing-resource-limited networks, the reduction in the energy allocated to step 2 is not conducive to the accuracy of target sensing. Therefore, the integrated scheme is more suitable for sensing-resource-limited networks. Finally, due to the spatial cooperation between radar positioning and target sensing, the accuracy of radar positioning can affect the accuracy of target sensing, resulting in the trade-off mentioned above.

### 5.2.2. Dual-Slot Networks

For the dual-slot synchronous ISAL networks, as shown in Figure 10, we give the sensing SPEB of the step-by-step and the integrated schemes in the four networks with different topologies in Figure 8.

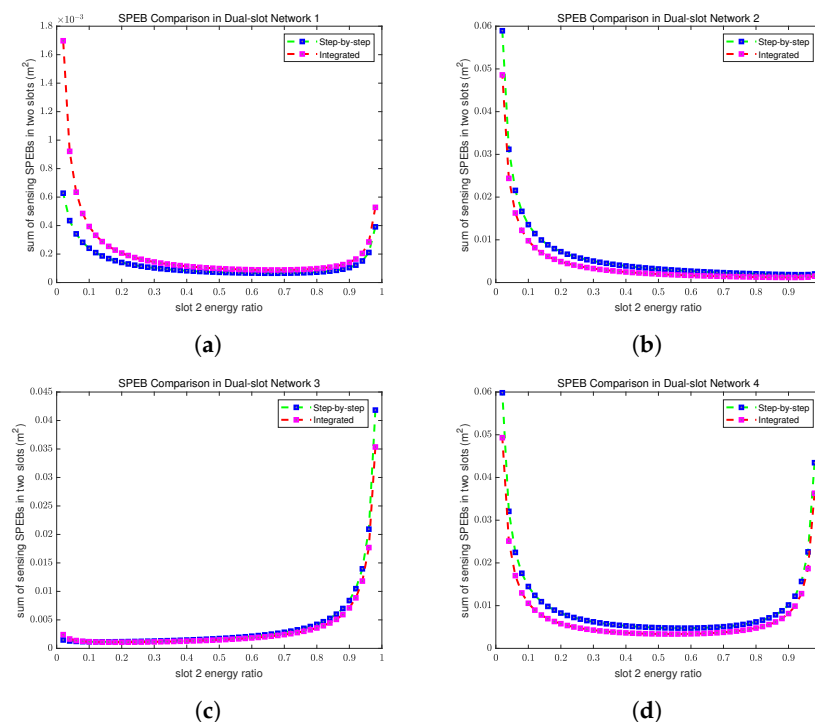


**Figure 10.** SPEB comparison between the step-by-stepscheme and the integrated scheme in four dual-slot synchronous networks. (a) SPEB comparison in a dual-slot synchronous network (Figure 8a). (b) SPEB comparison in a dual-slot synchronous network (Figure 8b). (c) SPEB comparison in a dual-slot synchronous network (Figure 8c). (d) SPEB comparison in a dual-slot synchronous network (Figure 8d).

According to Figure 10, we can draw the following conclusions. When the topologies of the partial networks used for target sensing in the two slots are similar, such as the topologies shown in Figure 8a,d, the energy allocation between the two time slots tends to be equal, as shown in Figure 10a,d. When there is a significant difference in the topologies of the partial networks used for target sensing in the two time slots, as shown in Figure 8b,c, more energy is allocated to the time slot corresponding to the sensing-resource-limited network, as shown in Figure 10b,c.

### 5.3. Asynchronous Networks

#### 5.3.1. Single-Slot Networks

For the single-slot asynchronous ISAL networks, due to the clock offset vector  $\tau$  in the parameter vectors to be estimated, when analyzing the energy optimization allocation between each step of the step-by-step scheme, we adopt the method of fixing the energy allocated to one parameter vector and analyzing the energy allocation relationship between the other two parameter vectors. For the asynchronous single-slot ISAL networks, as shown in Figure 11, we provide a comparison of the sensing SPEB results of the step-by-step scheme and the integrated scheme in the four networks with different topologies in Figure 7.

According to Figure 11, we have the following observations. Firstly, as shown in Figure 11a–d,m–p, when the energy allocated to step 2 is fixed, there is still a trade-off between localization and sensing. Moreover, when the network nodes are evenly distributed, the difficulty of target sensing is still much higher than that of radar positioning. From Figure 11e–h,q–t, it can be seen that, when the energy allocated to step 3 is fixed, the more energy allocated to step 1, the better the sensing accuracy. This means that, in the four single-slot asynchronous networks with different topologies, the difficulty of radar positioning is higher than that of estimating clock offset. Similarly, from Figure 11i–l,u–x, it can be seen that, when the energy allocated to step 1 is fixed, the more energy that is allocated to step 3, the better the sensing accuracy. This means that, in the four single-slot asynchronous networks with different topologies, the difficulty of target sensing is higher than that of estimating clock offset as well. In addition, similar to single-slot synchronous networks, in single-slot asynchronous networks, when the optimization objective function is the sensing SPEB, the step-by-step optimization scheme is more suitable for the sensing-resource-abundant network, as shown in Figure 11a–l. The integrated optimization scheme is more suitable for the sensing-resource-limited network, as shown in Figure 11m–x.

Based on the conclusion that the difficulty of estimating clock offset in the single-slot asynchronous networks is lower than that of radar positioning and target sensing, we give the following interpretation. As the example given in Appendix A, compared to (A1) and (A2), the elements of (A3) do not contain the coefficient  $\frac{1}{c}$ . Therefore, step 2 in which the clock offset is estimated in the step-by-step scheme requires less energy than the other two steps.

Above all, for the practical asynchronous ISAL networks with relatively uniform node distribution, in order to reduce the time complexity of the step-by-step scheme if adopted, we can set the energy allocated to each of the three steps in the step-by-step scheme as energy for clock offset < energy for radar localization < energy for target sensing, thereby reducing the time of traversal.

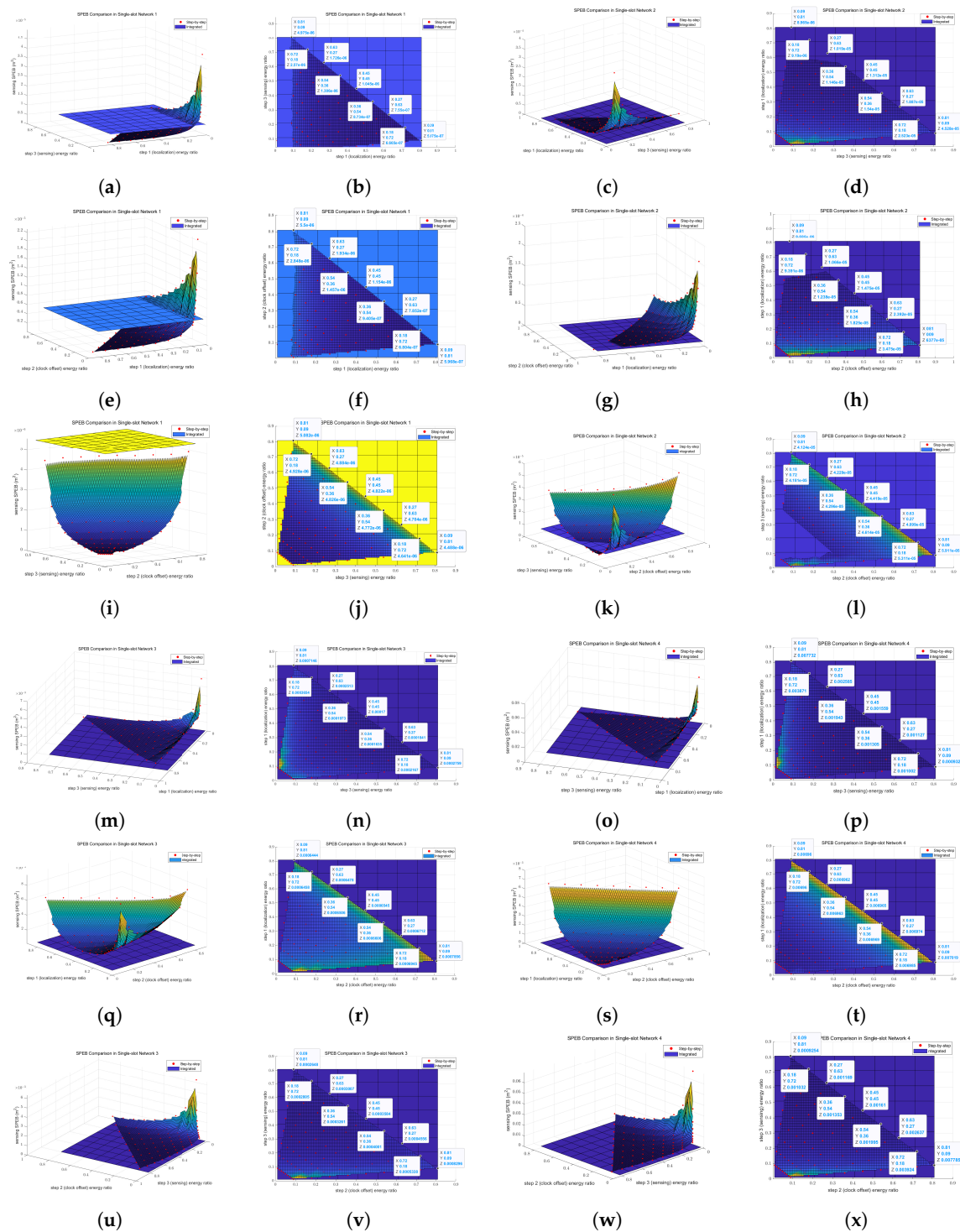


**Figure 11.** SPEB comparison between the step-by-step scheme and integrated scheme in four single-slot asynchronous networks. The images in the second and fourth columns are the plans of the stereograms in the first and third columns, respectively. (a,b,e,f,i,j) are, respectively, SPEB comparisons with step 2 energy, step 3 energy, and step 1 energy fixed in a single-slot asynchronous network (Figure 7a). (c,d,g,h,k,l) are, respectively, SPEB comparisons with step 2 energy, step 3 energy, and step 1 energy fixed in a single-slot asynchronous network (Figure 7b). (m,n,q,r,u,v) are, respectively, SPEB comparisons with step 2 energy, step 3 energy, and step 1 energy fixed in a single-slot asynchronous network (Figure 7c). (o,p,s,t,w,x) are, respectively, SPEB comparisons with step 2 energy, step 3 energy, and step 1 energy fixed in a single-slot asynchronous network (Figure 7d).

### 5.3.2. Dual-Slot Networks

For dual-slot asynchronous ISAL networks, as shown in Figure 12, we give the sensing SPEB of the step-by-step scheme and the integrated scheme in the four networks with different topologies in Figure 8.

It can be found from Figure 12 that the energy optimization allocation strategy between the two slots in the asynchronous networks is consistent with that in the synchronous networks.

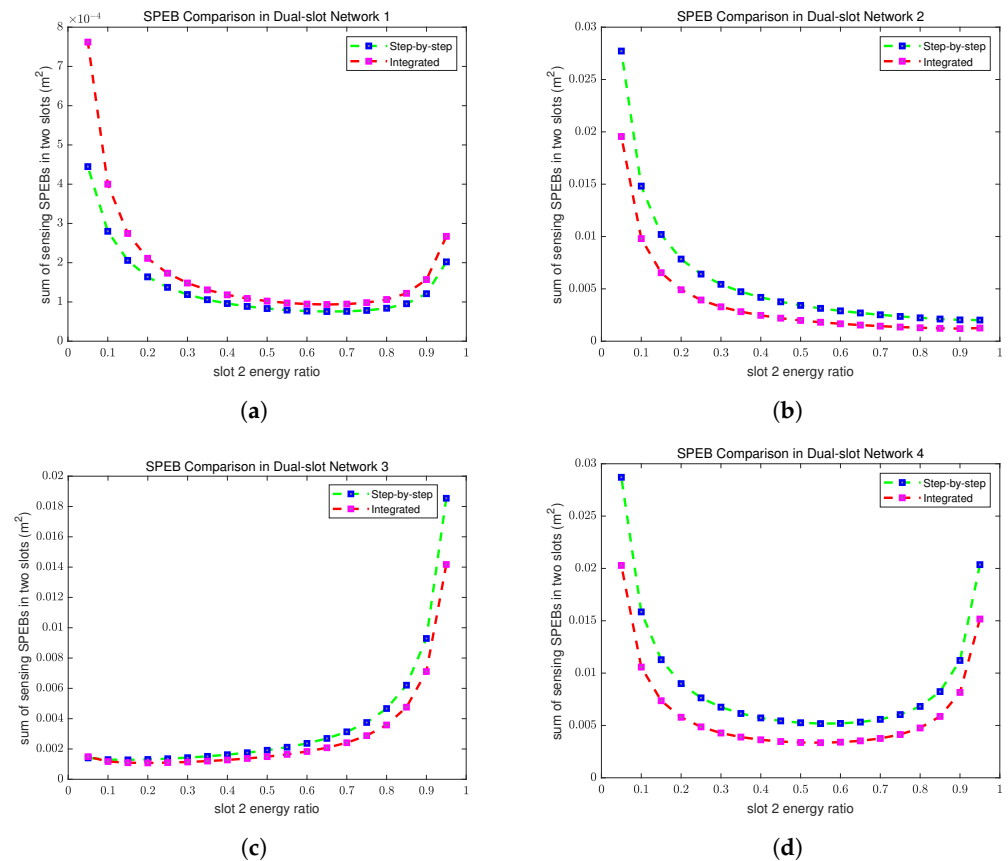


**Figure 12.** SPEB comparison between the step-by-step scheme and the integrated scheme in four dual-slot asynchronous networks. (a) SPEB comparison in a dual-slot asynchronous network (Figure 8a). (b) SPEB comparison in a dual-slot asynchronous network (Figure 8b). (c) SPEB comparison in a dual-slot asynchronous network (Figure 8c). (d) SPEB comparison in a dual-slot asynchronous network (Figure 8d).

### 6. Necessity of Using UWB Signals

In this section, we take the single-slot synchronous network shown in Figure 7c as an example and clarify the necessity of using UWB signals in the ISAL networks by comparing the SPEB results achieved with different signal bandwidths. We set the signal bandwidths to 500 MHz (UWB signal) and 5 MHz, respectively, and obtain the corresponding SPEBs, as shown in Figure 13.

It can be found from Figure 13 that the SPEB obtained by the 5 MHz signal is much larger than that obtained by the 500 MHz UWB signal. Therefore, to achieve high-precision sensing performance, there is a need to use UWB signals in the ISAL networks.



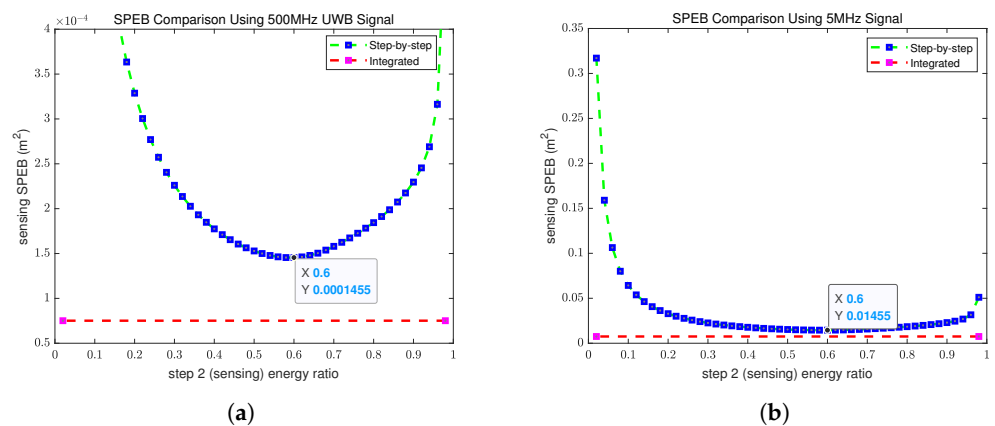


**Figure 13.** SPEB comparison between the step-by-step scheme and the integrated scheme using signals with different bandwidths. (a) Using a 500 MHz UWB signal. (b) Using a 5 MHz signal.

## 7. Conclusions and Future Work

In this article, we proposed single-slot and dual-slot ISAL network models and provide the derivation of fundamental limits in synchronous and asynchronous networks, respectively. For the optimization allocation of energy and power in the resource-constrained networks, this article proposed two optimization schemes—a step-by-step scheme and an integrated scheme—and provided solutions from the perspective of energy optimization allocation to solve the problem of the high time complexity of the step-by-step scheme. In addition, we also summarized the suitable scenarios for the step-by-step scheme and the integrated scheme by comparing the optimization results of networks with different topologies. From the simulation results, we drew the following regular conclusions: (i) in the sensing-resource-limited networks with uniformly distributed nodes, in order to reduce the time complexity of the step-by-step scheme, we can allocate energy for each step as energy for clock offset < energy for radar localization < energy for target sensing, thereby reducing the time of traversal; (ii) in the multi-slot ISAL networks, when optimizing the sum of sensing SPEBs in multiple time slots, more energy will be allocated to the sensing-resource-limited time slots; and (iii) the step-by-step optimization scheme is more suitable for the sensing-resource-abundant networks, while the integrated optimization scheme is more suitable for the sensing-resource-limited networks. The regular conclusions summarized in this article provide valuable theoretical references for resource allocation in practical ISAL networks.

For future study, there are mainly two research directions to extend. Firstly, in this article, our work only focuses on the theoretical simulation, aiming to demonstrate the theoretical feasibility of the proposed schemes, but it has not yet been validated in realistic environments through experiments. Secondly, the current state of the art of research in this area tends to introduce antenna array for radar positioning and target sensing. Its ability to simultaneously obtain TOA and AOA means it has higher positioning and sensing accuracy compared to the traditional single transmitter and receiver antennas. In this article, we only studied the fundamental limits and resource allocation schemes when each of the radars and anchors has a single transmitter and receiver antenna, but we have not yet extended our research to the antenna array. These two aspects are of great importance for further improving the work in this article.

**Author Contributions:** Conceptualization, R.Z., Y.B. and T.Z.; methodology, R.Z. and J.Y.; software, R.Z. and M.J.; validation, J.Y., Y.B. and T.Z.; formal analysis, R.Z. and J.Y.; investigation, R.Z. and M.J.; resources, Y.B.; data curation, R.Z.; writing—original draft preparation, R.Z.; writing—review and editing, R.Z., T.Z., J.Y., M.J. and Y.B.; visualization, R.Z.; supervision, T.Z. and Y.B.; project administration, T.Z.; funding acquisition, Y.B. All authors have read and agreed to the published version of the manuscript.



**Funding:** This paper was supported by the Natural Science Foundation of China under Grant No. 62171160, and the Fundamental Research Funds for the Central Universities under Grant No. HIT. OCEF. 2022055, and the Shenzhen Science and Technology Program under Grant No. KJZD20231023093055002, No. KJZD20230923114804009 and ZDSYS20210623091808025, and also major project of PCL.

**Institutional Review Board Statement:** Not applicable.

**Informed Consent Statement:** Not applicable.

**Data Availability Statement:** The data presented in this study are available on request from the corresponding author. The data are not publicly available due to restrictions of privacy.

**Conflicts of Interest:** Author Yachuan Bao was employed by the company The 54th Research Institute of China Electronics Technology Group Corporation. The remaining authors declare that the research was conducted in the absence of any commercial or financial relationships that could be construed as a potential conflict of interest.

## Appendix A. Partial Derivative Matrices Derivation

### Appendix A.1. Synchronous Networks

Taking a synchronous ISAL network containing two radars (numbered 1 and 2), two anchors (numbered 3 and 4), and one target (denoted as *tar*) as an example, we give the expressions of  $\frac{\partial \gamma}{\partial \mathbf{p}_r}$  and  $\frac{\partial \gamma}{\partial \mathbf{p}_t}$  as (A1) and (A2).

$$\frac{\partial \gamma}{\partial \mathbf{p}_r} = \begin{bmatrix} \frac{\partial \tau_{1,1}^{\text{sen}}}{\partial x_1} & \frac{\partial \tau_{1,1}^{\text{sen}}}{\partial y_1} & \frac{\partial \tau_{1,1}^{\text{sen}}}{\partial x_2} & \frac{\partial \tau_{1,1}^{\text{sen}}}{\partial y_2} \\ \vdots & \vdots & \vdots & \vdots \\ \frac{\partial \tau_{4,4}^{\text{sen}}}{\partial x_1} & \frac{\partial \tau_{4,4}^{\text{sen}}}{\partial y_1} & \frac{\partial \tau_{4,4}^{\text{sen}}}{\partial x_2} & \frac{\partial \tau_{4,4}^{\text{sen}}}{\partial y_2} \\ \frac{\partial \tau_{1,2}^{\text{ran}}}{\partial x_1} & \frac{\partial \tau_{1,2}^{\text{ran}}}{\partial y_1} & \frac{\partial \tau_{1,2}^{\text{ran}}}{\partial x_2} & \frac{\partial \tau_{1,2}^{\text{ran}}}{\partial y_2} \\ \vdots & \vdots & \vdots & \vdots \\ \frac{\partial \tau_{4,2}^{\text{ran}}}{\partial x_1} & \frac{\partial \tau_{4,2}^{\text{ran}}}{\partial y_1} & \frac{\partial \tau_{4,2}^{\text{ran}}}{\partial x_2} & \frac{\partial \tau_{4,2}^{\text{ran}}}{\partial y_2} \end{bmatrix}_{26 \times 4} = \begin{bmatrix} \frac{2 \cos(\varphi_{\text{tar},1})}{c} & \frac{2 \sin(\varphi_{\text{tar},1})}{c} & 0 & 0 \\ \frac{\cos(\varphi_{\text{tar},1})}{c} & \frac{\sin(\varphi_{\text{tar},1})}{c} & \frac{\cos(\varphi_{\text{tar},2})}{c} & \frac{\sin(\varphi_{\text{tar},2})}{c} \\ \frac{\cos(\varphi_{\text{tar},1})}{c} & \frac{\sin(\varphi_{\text{tar},1})}{c} & 0 & 0 \\ \frac{\cos(\varphi_{\text{tar},1})}{c} & \frac{\sin(\varphi_{\text{tar},1})}{c} & 0 & 0 \\ \frac{\cos(\varphi_{\text{tar},1})}{c} & \frac{\sin(\varphi_{\text{tar},1})}{c} & \frac{\cos(\varphi_{\text{tar},2})}{c} & \frac{\sin(\varphi_{\text{tar},2})}{c} \\ 0 & 0 & \frac{2 \cos(\varphi_{\text{tar},2})}{c} & \frac{2 \sin(\varphi_{\text{tar},2})}{c} \\ 0 & 0 & \frac{\cos(\varphi_{\text{tar},2})}{c} & \frac{\sin(\varphi_{\text{tar},2})}{c} \\ 0 & 0 & \frac{\cos(\varphi_{\text{tar},2})}{c} & \frac{\sin(\varphi_{\text{tar},2})}{c} \\ \frac{\cos(\varphi_{\text{tar},1})}{c} & \frac{\sin(\varphi_{\text{tar},1})}{c} & 0 & 0 \\ 0 & 0 & \frac{\cos(\varphi_{\text{tar},2})}{c} & \frac{\sin(\varphi_{\text{tar},2})}{c} \\ 0 & 0 & 0 & 0 \\ 0 & 0 & 0 & 0 \\ 0 & 0 & 0 & 0 \\ \frac{\cos(\varphi_{\text{tar},1})}{c} & \frac{\sin(\varphi_{\text{tar},1})}{c} & 0 & 0 \\ 0 & 0 & \frac{\cos(\varphi_{\text{tar},2})}{c} & \frac{\sin(\varphi_{\text{tar},2})}{c} \\ 0 & 0 & 0 & 0 \\ 0 & 0 & 0 & 0 \\ \frac{\cos(\varphi_{2,1})}{c} & \frac{\sin(\varphi_{2,1})}{c} & \frac{\cos(\varphi_{1,2})}{c} & \frac{\sin(\varphi_{1,2})}{c} \\ \frac{\cos(\varphi_{3,1})}{c} & \frac{\sin(\varphi_{3,1})}{c} & 0 & 0 \\ \frac{\cos(\varphi_{4,1})}{c} & \frac{\sin(\varphi_{4,1})}{c} & 0 & 0 \\ \frac{\cos(\varphi_{2,1})}{c} & \frac{\sin(\varphi_{2,1})}{c} & \frac{\cos(\varphi_{1,2})}{c} & \frac{\sin(\varphi_{1,2})}{c} \\ 0 & 0 & \frac{\cos(\varphi_{3,2})}{c} & \frac{\sin(\varphi_{3,2})}{c} \\ 0 & 0 & \frac{\cos(\varphi_{4,2})}{c} & \frac{\sin(\varphi_{4,2})}{c} \\ \frac{\cos(\varphi_{3,1})}{c} & \frac{\sin(\varphi_{3,1})}{c} & 0 & 0 \\ 0 & 0 & \frac{\cos(\varphi_{3,2})}{c} & \frac{\sin(\varphi_{3,2})}{c} \\ \frac{\cos(\varphi_{4,1})}{c} & \frac{\sin(\varphi_{4,1})}{c} & 0 & 0 \\ 0 & 0 & \frac{\cos(\varphi_{4,2})}{c} & \frac{\sin(\varphi_{4,2})}{c} \end{bmatrix} \quad (\text{A1})$$

$$\frac{\partial \gamma}{\partial \mathbf{p}_t} = \begin{bmatrix} \frac{\partial \tau_{1,1}^{\text{sen}}}{\partial x_{tar}} & \frac{\partial \tau_{1,1}^{\text{sen}}}{\partial y_{tar}} \\ \vdots & \vdots \\ \frac{\partial \tau_{4,4}^{\text{sen}}}{\partial x_{tar}} & \frac{\partial \tau_{4,4}^{\text{sen}}}{\partial y_{tar}} \\ \frac{\partial \tau_{1,2}^{\text{ran}}}{\partial x_{tar}} & \frac{\partial \tau_{1,2}^{\text{ran}}}{\partial y_{tar}} \\ \vdots & \vdots \\ \frac{\partial \tau_{4,2}^{\text{ran}}}{\partial x_{tar}} & \frac{\partial \tau_{4,2}^{\text{ran}}}{\partial y_{tar}} \end{bmatrix}_{26 \times 2} = \begin{bmatrix} \frac{2 \cos(\varnothing_{1,tar})}{c} & \frac{2 \sin(\varnothing_{1,tar})}{c} \\ \frac{\cos(\varnothing_{1,tar}) + \cos(\varnothing_{2,tar})}{c} & \frac{\sin(\varnothing_{1,tar}) + \sin(\varnothing_{2,tar})}{c} \\ \frac{\cos(\varnothing_{1,tar}) + \cos(\varnothing_{3,tar})}{c} & \frac{\sin(\varnothing_{1,tar}) + \sin(\varnothing_{3,tar})}{c} \\ \frac{\cos(\varnothing_{1,tar}) + \cos(\varnothing_{4,tar})}{c} & \frac{\sin(\varnothing_{1,tar}) + \sin(\varnothing_{4,tar})}{c} \\ \frac{\cos(\varnothing_{1,tar}) + \cos(\varnothing_{2,tar})}{c} & \frac{\sin(\varnothing_{1,tar}) + \sin(\varnothing_{2,tar})}{c} \\ \frac{2 \cos(\varnothing_{2,tar})}{c} & \frac{2 \sin(\varnothing_{2,tar})}{c} \\ \frac{\cos(\varnothing_{2,tar}) + \cos(\varnothing_{3,tar})}{c} & \frac{\sin(\varnothing_{2,tar}) + \sin(\varnothing_{3,tar})}{c} \\ \frac{\cos(\varnothing_{2,tar}) + \cos(\varnothing_{4,tar})}{c} & \frac{\sin(\varnothing_{2,tar}) + \sin(\varnothing_{4,tar})}{c} \\ \frac{\cos(\varnothing_{1,tar}) + \cos(\varnothing_{3,tar})}{c} & \frac{\sin(\varnothing_{1,tar}) + \sin(\varnothing_{3,tar})}{c} \\ \frac{\cos(\varnothing_{2,tar}) + \cos(\varnothing_{3,tar})}{c} & \frac{\sin(\varnothing_{2,tar}) + \sin(\varnothing_{3,tar})}{c} \\ \frac{2 \cos(\varnothing_{3,tar})}{c} & \frac{2 \sin(\varnothing_{3,tar})}{c} \\ \frac{\cos(\varnothing_{3,tar}) + \cos(\varnothing_{4,tar})}{c} & \frac{\sin(\varnothing_{3,tar}) + \sin(\varnothing_{4,tar})}{c} \\ \frac{\cos(\varnothing_{1,tar}) + \cos(\varnothing_{4,tar})}{c} & \frac{\sin(\varnothing_{1,tar}) + \sin(\varnothing_{4,tar})}{c} \\ \frac{\cos(\varnothing_{2,tar}) + \cos(\varnothing_{4,tar})}{c} & \frac{\sin(\varnothing_{2,tar}) + \sin(\varnothing_{4,tar})}{c} \\ \frac{\cos(\varnothing_{3,tar}) + \cos(\varnothing_{4,tar})}{c} & \frac{\sin(\varnothing_{3,tar}) + \sin(\varnothing_{4,tar})}{c} \\ \frac{2 \cos(\varnothing_{4,tar})}{c} & \frac{2 \sin(\varnothing_{4,tar})}{c} \\ 0 & 0 \\ 0 & 0 \\ 0 & 0 \\ 0 & 0 \\ 0 & 0 \\ 0 & 0 \\ 0 & 0 \\ 0 & 0 \\ 0 & 0 \\ 0 & 0 \end{bmatrix} \quad (A2)$$

#### Appendix A.2. Asynchronous Networks

Taking an asynchronous ISAL network containing two radars (numbered 1 and 2), two anchors (numbered 3 and 4), and one target (denoted as *tar*) as an example,  $\boldsymbol{\tau} = [\tau_{1,2}, \tau_{1,3}]^T$ ,  $\frac{\partial \zeta}{\partial \mathbf{p}_r}$ , and  $\frac{\partial \zeta}{\partial \mathbf{p}_t}$  are expressed as (A1) and (A2). We give the expression of  $\frac{\partial \zeta}{\partial \boldsymbol{\tau}}$  as (A3).

$$\frac{\partial \zeta}{\partial \tau} = \begin{bmatrix} \frac{\partial \zeta_{1,1}^{\text{sen}}}{\partial \tau_{1,2}} & \frac{\partial \zeta_{1,1}^{\text{sen}}}{\partial \tau_{1,3}} \\ \vdots & \vdots \\ \frac{\partial \zeta_{4,4}^{\text{sen}}}{\partial \tau_{1,2}} & \frac{\partial \zeta_{4,4}^{\text{sen}}}{\partial \tau_{1,3}} \\ \frac{\partial \zeta_{1,2}^{\text{ran}}}{\partial \tau_{1,2}} & \frac{\partial \zeta_{1,2}^{\text{ran}}}{\partial \tau_{1,3}} \\ \vdots & \vdots \\ \frac{\partial \zeta_{4,2}^{\text{ran}}}{\partial \tau_{1,2}} & \frac{\partial \zeta_{4,2}^{\text{ran}}}{\partial \tau_{1,3}} \end{bmatrix}_{26 \times 2} = \begin{bmatrix} 0 & 0 \\ 1 & 0 \\ 0 & 1 \\ 0 & 1 \\ -1 & 0 \\ 0 & 0 \\ -1 & 1 \\ -1 & 1 \\ 0 & -1 \\ 1 & -1 \\ 0 & 0 \\ 0 & 0 \\ 0 & -1 \\ 1 & -1 \\ 0 & 0 \\ 0 & 0 \\ 1 & 0 \\ 0 & 1 \\ 0 & 1 \\ -1 & 0 \\ -1 & 1 \\ -1 & 1 \\ 0 & -1 \\ 1 & -1 \\ 0 & -1 \\ 1 & -1 \end{bmatrix} \quad (\text{A3})$$

## References

1. Zhao, H.; Zhang, Z.; Wang, J.; Zhang, Z.; Shen, Y. A Signal-Multiplexing Ranging Scheme for Integrated Localization and Sensing. *IEEE Wirel. Commun. Lett.* **2022**, *11*, 1609–1613. [\[CrossRef\]](#)
2. Zhang, H.; Zhang, T.; Shen, Y. Modulation Symbol Cancellation for OTFS-Based Joint Radar and Communication. In Proceedings of the 2021 IEEE International Conference on Communications Workshops (ICC Workshops), Virtual, 14–23 June 2021; pp. 1–6.
3. Shen, Y.; Win, M.Z. On the accuracy of localization systems using wideband antenna arrays. *IEEE Trans. Commun.* **2010**, *58*, 270–280. [\[CrossRef\]](#)
4. Wang, P.; Morton, Y.J. Multipath Estimating Delay Lock Loop for LTE Signal TOA Estimation in Indoor and Urban Environments. *IEEE Trans. Wirel. Commun.* **2020**, *19*, 5518–5530. [\[CrossRef\]](#)
5. Laoudias, C.; Moreira, A.; Kim, S.; Lee, S.; Wirola, L.; Fischione, C. A Survey of Enabling Technologies for Network Localization, Tracking, and Navigation. *IEEE Commun. Surv. Tutorials* **2018**, *20*, 3607–3644. [\[CrossRef\]](#)
6. Zafari, F.; Gkelias, A.; Leung, K.K. A Survey of Indoor Localization Systems and Technologies. *IEEE Commun. Surv. Tutorials* **2019**, *21*, 2568–2599. [\[CrossRef\]](#)
7. Gezici, S.; Tian, Z.; Giannakis, G.; Kobayashi, H.; Molisch, A.; Poor, H.; Sahinoglu, Z. Localization via ultra-wideband radios: A look at positioning aspects for future sensor networks. *IEEE Signal Process. Mag.* **2005**, *22*, 70–84. [\[CrossRef\]](#)
8. An, D.J.; Lee, J.H. Derivation of an Approximate Location Estimate in Angle-of-Arrival Based Localization in the Presence of Angle-of-Arrival Estimate Error and Sensor Location Error. In Proceedings of the 2018 IEEE World Symposium on Communication Engineering (WSCE), Singapore, 28–30 December 2018; pp. 1–5. [\[CrossRef\]](#)
9. Pavani, T.; Costa, G.; Mazzotti, M.; Conti, A.; Dardari, D. Experimental Results on Indoor Localization Techniques through Wireless Sensors Network. In Proceedings of the 2006 IEEE 63rd Vehicular Technology Conference, Melbourne, Australia, 7–10 May 2006; Volume 2, pp. 663–667. [\[CrossRef\]](#)
10. Xu, Y.; Zhou, J.; Zhang, P. RSS-Based Source Localization When Path-Loss Model Parameters are Unknown. *IEEE Commun. Lett.* **2014**, *18*, 1055–1058. [\[CrossRef\]](#)
11. Zheng, Z.; Hua, J.; Wu, Y.; Wen, H.; Meng, L. Time of arrival and Time Sum of arrival based NLOS identification and localization. In Proceedings of the 2012 IEEE 14th International Conference on Communication Technology, Chengdu, China, 9–11 November 2012; pp. 1129–1133. [\[CrossRef\]](#)
12. Zheng, X.; Hua, J.; Zheng, Z.; Peng, H.; Meng, L. Wireless localization based on the time sum of arrival and Taylor expansion. In Proceedings of the 2013 19th IEEE International Conference on Networks (ICON), Singapore, 11–13 December 2013; pp. 1–4. [\[CrossRef\]](#)

13. Poulouse, A.; Emersic, Z.; Steven Eyobu, O.; Seog Han, D. An Accurate Indoor User Position Estimator For Multiple Anchor UWB Localization. In Proceedings of the 2020 International Conference on Information and Communication Technology Convergence (ICTC), Jeju, Republic of Korea, 21–23 October 2020; pp. 478–482. [\[CrossRef\]](#)
14. Win, M.Z.; Shen, Y.; Dai, W. A Theoretical Foundation of Network Localization and Navigation. *Proc. IEEE* **2018**, *106*, 1136–1165. [\[CrossRef\]](#)
15. Wymeersch, H.; Seco-Granados, G. Radio Localization and Sensing-Part I: Fundamentals. *IEEE Commun. Lett.* **2022**, *26*, 2816–2820. [\[CrossRef\]](#)
16. Larsson, E. Cramer-Rao bound analysis of distributed positioning in sensor networks. *IEEE Signal Process. Lett.* **2004**, *11*, 334–337. [\[CrossRef\]](#)
17. Shen, Y.; Win, M.Z. Fundamental Limits of Wideband Localization- Part I: A General Framework. *IEEE Trans. Inf. Theory* **2010**, *56*, 4956–4980. [\[CrossRef\]](#)
18. Shen, Y.; Wymeersch, H.; Win, M.Z. Fundamental Limits of Wideband Localization- Part II: Cooperative Networks. *IEEE Trans. Inf. Theory* **2010**, *56*, 4981–5000. [\[CrossRef\]](#)
19. Guan, Y.; Deng, J.; Cheng, X. On the Accuracy of Wideband Localization in Quantized Uplink Massive MIMO Systems. *IEEE Commun. Lett.* **2022**, *26*, 1558–1562. [\[CrossRef\]](#)
20. Chaccour, C.; Soorki, M.N.; Saad, W.; Bennis, M.; Popovski, P.; Debbah, M. Seven Defining Features of Terahertz (THz) Wireless Systems: A Fellowship of Communication and Sensing. *IEEE Commun. Surv. Tutorials* **2022**, *24*, 967–993. [\[CrossRef\]](#)
21. Liu, C.; Fang, D.; Yang, Z.; Jiang, H.; Chen, X.; Wang, W.; Xing, T.; Cai, L. RSS Distribution-Based Passive Localization and Its Application in Sensor Networks. *IEEE Trans. Wirel. Commun.* **2016**, *15*, 2883–2895. [\[CrossRef\]](#)
22. Xiao, J.; Wu, K.; Yi, Y.; Wang, L.; Ni, L.M. Pilot: Passive Device-Free Indoor Localization Using Channel State Information. In Proceedings of the 2013 IEEE 33rd International Conference on Distributed Computing Systems, Philadelphia, PA, USA, 8–11 July 2013; pp. 236–245. [\[CrossRef\]](#)
23. Shen, Y.; Dai, W.; Win, M.Z. Power Optimization for Network Localization. *IEEE/ACM Trans. Netw.* **2014**, *22*, 1337–1350. [\[CrossRef\]](#)
24. Li, W.W.L.; Shen, Y.; Zhang, Y.J.; Win, M.Z. Robust power allocation via semidefinite programming for wireless localization. In Proceedings of the 2012 IEEE International Conference on Communications (ICC), Ottawa, ON, Canada, 10–15 June 2012; pp. 3595–3599.
25. Jia, M.; Yang, J.; Zhang, T. Power Allocation in Infrastructure Limited Integration Sensing and Localization Wireless Networks. In Proceedings of the 2022 IEEE 96th Vehicular Technology Conference (VTC2022-Fall), London, UK, 26–29 September 2022; pp. 1–5.
26. Zhang, R.; Yang, J.; Zhang, T. Resource Optimization in Time-Varying Wireless Sensing and Localization Networks. In Proceedings of the 2023 IEEE 97th Vehicular Technology Conference (VTC2023-Spring), Florence, Italy, 20–23 June 2023; pp. 1–6. [\[CrossRef\]](#)
27. Zhang, T.; Molisch, A.F.; Shen, Y.; Zhang, Q.; Feng, H.; Win, M.Z. Joint Power and Bandwidth Allocation in Wireless Cooperative Localization Networks. *IEEE Trans. Wirel. Commun.* **2016**, *15*, 6527–6540. [\[CrossRef\]](#)

**Disclaimer/Publisher’s Note:** The statements, opinions and data contained in all publications are solely those of the individual author(s) and contributor(s) and not of MDPI and/or the editor(s). MDPI and/or the editor(s) disclaim responsibility for any injury to people or property resulting from any ideas, methods, instructions or products referred to in the content.